İSTANBUL TECHNICAL UNIVERSITY ★ ENERGY INSTITUTE

CRYSTAL STRUCTURE PREDICTION AND AMMONIA DYNAMICS IN CALCIUM AMMINE

M.Sc. THESIS

Sencer BÜYÜKYEĞEN

Energy Science and Technology Division

Energy Science and Technology Programme

JUNE 2017

İSTANBUL TECHNICAL UNIVERSITY ★ ENERGY INSTITUTE

CRYSTAL STRUCTURE PREDICTION AND AMMONIA DYNAMICS IN CALCIUM AMMINE

M.Sc. THESIS

Sencer BÜYÜKYEĞEN
(301131025)

Energy Science and Technology Division

Energy Science and Technology Programme

Thesis Advisor: Assoc. Prof. Dr. Adem TEKİN

JUNE 2017

İSTANBUL TEKNİK ÜNİVERSİTESİ ★ ENERJİ ENSTİTÜSÜ

KALSİYUM AMİNİN KRİSTAL YAPI TAHMİNİ VE AMONYAK DİNAMİĞİNİN İNCELENMESİ

YÜKSEK LİSANS TEZİ

Sencer BÜYÜKYEĞEN
(301131025)

Enerji Bilim ve Teknoloji Anabilim Dalı

Enerji Bilim ve Teknoloji Programı

Tez Danışmanı: Doç. Dr. Adem TEKİN

HAZİRAN 2017

Sencer Büyükyeğen, a M.Sc. student of İTU Institute of Energy 301131025, successfully defended the thesis/dissertation entitled "CRYSTAL STRUCTURE PREDICTION AND AMMONIA DYNAMICS IN CALCIUM AMMINE", which he prepared after fulfilling the requirements specified in the associated legislations, before the jury whose signatures are below.

Thesis Advisor :	**Assoc. Prof. Dr. Adem TEKİN** İstanbul Technical University	.....
Jury Members :	**Prof. Dr. Nilgün KARATEPE YAVUZ** İstanbul Technical University	.....
	Assoc. Prof. Dr. Hikmet Hakan GÜREL Kocaeli University	.....

Date of Submission : 03 May 2017
Date of Defense : 06 June 2017

To my beloved parents,

FOREWORD

This master thesis, which covers a scientific research project, was done under the supervision of my thesis adviser Assoc. Prof. Dr. Adem TEKİN.

The aim of this thesis, as is understood from the title, was to make predictions for the crystal structure of the Calcium Metal Ammine Complexes as well as understand ammonia desorption and absorbtion mechanism of these materials.

I would like to state that it is a great honour for me to work under the guidance of my thesis advisor Assoc. Prof. Dr. Adem TEKİN, thanks for being an excellent mentor and a great inspiration to me and many thanks for your patience. I also would like to thank my friends for encouraging me in this work, last and most importantly my parents for their support and understanding within this period. Lastly I would like to express my appreciation to the Department of Scientific Research Projects (BAP) of Istanbul Technical University for their support.

May 2017

Sencer BÜYÜKYEĞEN
(Physics Engineer)

TABLE OF CONTENTS

Page

ABBREVIATIONS

CASPESA : Crystal Structure Prediction via Simmulated Annealing
CPU : Central Processing Unit
DET : Dürtülü Elastik Takım
DFT : Density Functional Theory
DTU : Technical University of Denmark
HF : Hartree-Fock
HF-SCF : Hartree-Fock Self Consistent Field
IEO : International Energy Outlook
IRENA : The International Renewable Energy Agency
MEP : Minimum Energy Path
NEB : Nudged Elastic Band
PEMFCs : Polymer Electrolyte Membrane Fuel Cells
RPBE : Revised Perdew-Burke-Ernzerhof Functional
SOFC : Solid Oxide Fuel Cell
YFT : Yoğunluk Fonksiyon Teorisi

LIST OF TABLES

Page

LIST OF FIGURES

Page

CRYSTAL STRUCTURE PREDICTION AND AMMONIA DYNAMICS IN CALCIUM AMMINE

SUMMARY

In today's world of decreasing fossil fuel supplies by contrast with growing population and requisite for energy, hydrogen as being one of the renewable energy sources, is important and alternative energy carrier for meeting this increasing energy demand.

Hydrogen has a high energy efficiency and rich source. Furthermore, it is unpolluted and eco-friendly fuel which has no carbon emission. Thus, it is getting more important everyday among other energy sources.

Despite having all those advantages, storage causes huge problem as compared to the other fuel types. It is possible to store, transport and use hydrogen both in gas and liquid phases. However, storing hydrogen in the gas phase requires quite large volumes. Storing in the liquid phase needs high pressures and therefore some of the produced energy should be used for liquefaction process which ultimately causes an increase in total cost. In the solid phase, hydrogen can be much more easily and safely stored as compared to previously mentioned phases, nevertheless, there is no excellent reported material capable of fast and reversible hydrogen absorption and desorption.

It is also possible to store hydrogen indirectly (not as H_2). Especially metal ammines, which include ammonia, have better storage characteristics than other direct and indirect materials. They have fast and reversible ammonia absorption and desorption characteristics as well as higher volumetric hydrogen densities. Desorption of ammonia from metal ammines is easy and only limited by heat transportation.

When determining the most appropriate metal ammine, it is also required to take weight, price and volume parameters into consideration. One of those alkaline earth metal is magnesium and due to having low pressure and high gravimetric capacity, $Mg(NH_3)_6Cl_2$ (9.19 wt% hydrogen) is the most examined metal ammine in the literature. Calcium metal ammine, on the other hand, is an other alternative medium requiring much lower temperatures for the desorption of ammonia compared to magnesium complex. $Ca(NH_3)_8Cl_2$ (9.78 wt% hydrogen) can emit six ammonia molecules at 360K (for the first four ammonia molecules at around 320K).

Experimentally only the crystal structures of octa- and diammine calcium complexes have been reported. In order to study the ammonia dynamics in all complexes ($Ca(NH_3)_nCl_2$ with n=8,6,4,2,1), knowledge about their crystal structures is a necessity. Therefore, this study first predicts the crystal structures of all calcium ammine complexes by using an algorithm based on simulating annealing and density functional theory methods, called as CASPESA. With the help of promising stable (verified by phonon calculations) structures obtained from CASPESA, ammonia dynamics in these complexes were investigated by using minimum energy path techniques and the density functional level of theory. Global crystal structure optimizations carried out with CASPESA yielded new crystal structures lower in energy than the experimental ones for all ammonia content (n=8,6,4,2,1). The

subsequent treatment of these newly found structures in the nudged elastic band calculations led to ammonia migration paths requiring close to the experimental desorption enthalpies. This indicates that ammonia mobility in these complexes might be limited to bulk diffusion.

KALSİYUM AMİNİN KRİSTAL YAPI TAHMİNİ VE AMONYAK DİNAMİĞİNİN İNCELENMESİ

ÖZET

Günümüz dünyasının enerji ihtiyacanın önemli bir bölümünü karşılayan fosil yakıt rezervlerinin giderek azalması, buna karşın hızla artmaya devam eden nüfus ve buna bağlı olarak enerji talebi, dünyada yeni enerji kaynaklarına yönelimi zorunlu kılmaktadır. Halihazırda, fosil yakıtların atmosfere yaydığı CO_2 ve diğer sera gazları insan sağlığına zararlı etkisinin yanı sıra iklim değişikliğine de neden olduğu bilinmektedir. Bu yüzden mevcut enerji kaynaklarının verimli kullanılması büyük önem taşımaktadır. Ayrıca doğal kaynaklardan elde edilen ve sürdürülebilirliği olan güneş, rüzgar, biyokütle, jeotermal, hidrolik, hidrojen, dalga enerjisi gibi alternatif enerji kaynakları teşvik edilirken, günümüzde bu kaynaklardan enerji elde edilmesindeki maliyet-verim dengesini gözeten yeni teknolojiler geliştirilmektedir.

Hidrojen; yüksek verimliliğe sahip, kaynağı bol, kullanımı temiz, çevreyi kirletici ve sera etkisini artırıcı karbondioksit salınımı veya benzeri gaz ve zararlı kimyasal madde üretimi söz konusu olmayan, çevre dostu bir enerji taşıyıcısı olması sebebiyle yenilenebilir enerji kaynakları arasında önemi her geçen gün artmaktadır.

Bütün bu avantajlarına rağmen, hidrojenin üretimi, depolanması, ve günlük kullanımı diğer enerji kaynaklarına göre problem yaratmaktadır. Hidrojenin gaz veya sıvı fazda saklanması, taşınması ve kullanımı mümkündür. Ancak gaz fazda depoloma ve kullanımı çok büyük hacimler gerektirmektedir. Sıvı olarak depolama ise yüksek basınçlar altında çalışılmasını gerektirmekte ve hidrojen enerjisinin belirli bir bölümü sıvılaştırma işlemi için harcanmaktadır. Bu durum maliyeti arttıracağından yine elverişli bir çözüm getirmemektedir. Katı olarak depolanması diğer fazlara göre daha kolay ve güvenli bir çözüm sunması sebebiyle metal hidritler, karbon nanotüpler, metal-organik sistemler, metal borhidritler, amonyum boran gibi sistemler bu amaçla detaylı bir şekilde incelenmiştir. Ancak katı olarak depolama da hızlı, tersinir ve yüksek yoğunlukta hidrojen alımı ve salınımında iyi sonuçlar vermemektedir.

Hidrojenin dolaylı(endirekt) olarak depolanması da mümkündür. Hidrojene benzer şekilde karbon salınımı gerçekleşmeyen ve sera gazı olmayan amonyak, hidrojene alternatif bir enerji taşıyıcısı olma özelliği taşımaktadır. Amonyak halihazırda aşırı toksikliğinden ötürü yakıt olarak tercih edilmemektedir ancak amonyak metal aminlerde depolandığında standart basınç ve sıcaklıktaki sıvı amonyağa nazaran % 33 oranında daha az amonyak toksikliği görülmektedir. Böylece başlıca doğal gazdan üretilen amonyak, özellikle metal aminlerde depolandığında ulaşım sektörü için önemli bir potansiyel yakıt haline dönüşebilmektedir.

Metal aminler, diğer direkt ve endirekt malzemelere göre daha iyi depolama özellikleri göstermektedirler. Amonyak, katı halde metal aminlerde depolandığında, sıvı amonyak ve diğer metal hidrtilere göre hacimsel hidrojen yoğunluğu daha fazladır.

Ayrıca, metal hidritlere göre daha hafif olan bu malzemeler, hızlı ve tersinir bir amonyak alımı ve salınımına sahiptirler.

Metal aminler ile ilgili ilk araştırmalar Danimarka Teknik Üniversitesi kimya ve fizik bölümlerinde 2005 yılında gerçekleştirilmiştir. Bu çalışmada, $Mg(NH_3)_6Cl_2$ kompleksi hazırlanmış ve sıcaklık kontrollü salınım deneyleri yapılmıştır. Daha sonrasında, amonyağın $Mg(NH_3)_6Cl_2$ tuzundan salınımı ile meydana gelen gözenekler yine Danimarka Teknik Üniversitesi fizik ve kimya bölümlerindeki araştırmacılar tarafından incelenmiştir. $Mg(NH_3)_6Cl_2$ tuzunun ısısal parçalanması sırasındaki nano ölçekli yapı karakterizasyonu da X-ışını saçılımı tekniğiyle 2007 yılında yine benzer araştırmacılar tarafından gerçekleştirilmiştir. Bu çalışmada, magnezyum amin kompleksinin kristal yapısında yer alan boşlukların, $Mg(NH_3)_6Cl_2$'den $Mg(NH_3)_2Cl_2$' ye geçildiğinde % 5'den %55' e ve daha sonrasında $Mg(NH_3)Cl_2$' ye ulaşıldığında ise % 71'e vardığı bulunmuştur. Bu boşlukların oluşmasının nedeni, metal aminlerin hızlı amonyak absorpsiyonu yapmalarından kaynaklanmaktadır.

Endirekt hidrojen depoloama malzemelerinden biri olan metal amin tuzları sonraki süreçte AMMINEX firması tarafından geliştirilerek, tekrar doldurulabilen, otomobil ve kamyonlarda kullanılabilecek bir ürün haline dönüştürülmüştür. Katalizör yardımı ile % 80 verimle amonyak hidrojene dönüştürülüp, hidrojen polimer elektrolit membrane (PEM) yakıt pilinde yakılabilmektedir.

Enerji taşıyıcı olarak belirlenecek metal aminler için yüksek kütlesel hidrojen içeriği, hızlı ve tersinir amonyak desorpsiyon ve absorpsiyonu ve güvenlik gibi parametrelerinin yanı sıra kolay bulunabilir olması ve fiyat gibi etkenleri de göz önünde bulundurmak gerekir. Metal amin tuzları arasında, oda sıcaklığında sadece 2mbar gibi düşük bir basınca sahip olan, yüksek kütlesel (ağırlıkça % 9.19) ve hacimsel (109 (gH_2) L^{-1}) hidrojen içeriğiyle bir prototip olarak kabul edilen $Mg(NH_3)_6Cl_2$ (magnezyum hegza amin), literatürde üzerinde en fazla inceleme yapılan metal amin kompleksidir. Magnezyum hegza amin dışında, $Ca(NH_3)_8Cl_2$ (% 9.78 ağırlıkça hidrojen) ve $Sr(NH_3)_8Cl_2$ (% 8.21 ağırlıkça hidrojen) da diğer önemli metal aminlerdendir. Magnezyum amindeki hızlı amonyak alımı ve salınımı, amonyağın bu kompleksdeki kütlesel difüzyonundan kaynaklanabileceği bulunmuştur. $Mg(NH_3)_6Cl_2$ 440 K civarında dört molekül amonyak salınımı gerçekleştirirken, son iki amonyak molekülünü için ise 675 K gibi bir sıcaklık gerekmektedir. Ancak bu seviye, taşıtlar için erişilmesi zor bir sıcaklıktır.

Bir diğer taşıyıcı malzeme modeli olarak belirlenen $Ca(NH_3)_8Cl_2$ (% 9.78 ağırlıkça hidrojen) metal amini ise 360K civarında altı molekül amonyak (ilk dört molekül için 320K civarında olmak üzere) salabilmektedir. Ayrıca, $Ca(NH_3)_8Cl_2$ 300 K'deki amonyak buhar basıncı 0.77 bar olmaktadır. Bu iki metal amin tuzunun diğer bir avantajı da içerdikleri $MgCl_2$ ve $CaCl_2$ gibi tuzların ucuz ve bolca bulunmasıdır.

Bu çalışmada, yüksek hidrojen içeriği ve magnezyum metal amine kıyasla daha düşük sıcaklıklarda amonyak salınımının gerçekleştiği kalsiyum amin tuzu için hem kristal yapı tahmini hemde amonyak dinamikleri incelenmiştir. İlk olarak literatürdeki deneysel çalışmalar incelenmiş olup, sonrasında "Methods" bölümünde detaylı tanıtılmış olan benzetilmiş tavlama metoduna dayanan kristal yapı tahmin algoritması ile tüm $Ca(NH_3)nCl_2$ (n = 8, 6, 4, 2, 1) amin komplekslerinin kristal yapıları belirlenmiştir. Yoğunluk fonksiyon teorisi (YFT) metoduna dayalı düzlem dalga kodu olan DACAPO ile hem enerji hemde fonon (phonon) hesaplamaları yapılarak, hangi yapının en düşük enerjiye sahip ve kararlı olduğu bulunmuştur. Elde edilen kararlı yapılar deneysel verilerle karşılaştırılmış, ayrıca bu yapılardaki amonyak grubunun

davranışı, hızlı alınım ve salınım mekanizmaları, minimum enerji yolu hesaplama prensibine dayalı dürtülü elastik takım (DET) tekniği ile detaylıca incelenmiştir.

CASPESA ile küresel kristal yapı optimizasyonu sonucu elde edilen $Ca(NH_3)_nCl_2$ n = 8, 6, 4, 2, 1 kristal yapılarının, deneysel sonuçlara göre daha düşük enerjiye sahip olduğu görülmüştür. Beraberinde, dürtülü elastik takım tekniği ile söz konusu yeni yapılarda amonyak yayınım yolları için gereken desorpsiyon entalpi değerlerinin, deneysel verilere yakın sonuç verdiği hesaplanmıştır. Bu sonuç, kalsiyum amin komplekslerindeki amonyak difuzyonunun kitlesel (bulk) yayınımla sınırlı olabileceğini göstermektedir.

1. INTRODUCTION

1.1 Aims and Objectives

Metal ammine salts, one of the most important indirect hydrogen storage materials, can be transformed into such a form that they can be refilled in steel or aluminum cartridges for cars and trucks. This system has been invented and used by Amminex Emissions Technology, a fast growing Danish clean-tech Company, which is based on catalytic decomposition of ammonia yielding hydrogen with 80% efficiency. Moreover, $Mg(NH_3)_6Cl_2$, $Sr(NH_3)_8Cl_2$ and $Ca(NH_3)_8Cl_2$ metal ammine complexes are candidate materials for this kind of system, due to their low pressure and high gravimetric hydrogen capacity such as 9.78 wt% hydrogen for calcium octaammine.

Metal ammines have fast absorption and desorption ammonia kintecis. However, it is not known that how this process occurs at atomic level. The aim of this thesis is to investigate mechanism involved in these fast kinetic reactions.

For this purpose, a combined approach with crystal structure prediction based on simulated annealing (CASPESA) and density functional theory (DFT) has been employed $Ca(NH_3)_nCl_2$ n = 6, 4, 2, 1 complexes together with minimum energy path techniques, such as nudget elastic band method (NEB).

1.2 Literature Review

Although metal ammines have been known for a long time [1-5] (especially crystal structures and phase transformations of these complexes were investigated in these studies), it was the first in 2005 that they took place in the literature for the purpose of indirect hydrogen storage studies done by Christensen et al. [6]. In this study, $Mg(NH_3)_6Cl_2$ complex was prepared and temperature controlled desorption experiments were carried out. Subsequently, the pores that were formed by the desorption of ammonia from the $Mg(NH_3)_6Cl_2$ salt were again investigated by the same researchers [7].

In 2007, the nanoscale structure characterization of the thermal decomposition of the $Mg(NH_3)_6Cl_2$ salt was also performed by similar researchers with X-ray scattering technique [8]. Porosity ratio was found to increase from 5% to 55% and to 71% for the reactions $Mg(NH_3)_6Cl_2 \rightarrow Mg(NH_3)_2Cl_2 + 4NH_3$ and $Mg(NH_3)_2Cl_2 \rightarrow Mg(NH_3)Cl_2 + NH_3$, respectively. Those porosities are the reason for the fast ammonia absorption of metal ammines. Moreover, in 2008, the advantages and disadvantages ammonia for hydrogen storage was reported [9]. As it is well known that liquid ammonia is toxic and can be poisonous. Besides, there is still ammonia left sparingly after decomposition of that into hydrogen. Those two are the biggest handicaps for ammonia as an energy carrier.

Sørensen et al. [10] performed detailed study on the indirect hydrogen storage capabilities of $Mg(NH_3)_6Cl_2$, $Ca(NH_3)_8Cl_2$, $Mn(NH_3)_6Cl_2$ and $Ni(NH_3)_6Cl_2$ salts. According to this study, these four metal ammines can be compressed into solid pellets, which ultimately increases the volumetric and the gravimetric hydrogen density. Alongside with these four metal ammines, enthalpy values of ammonia desorption as well as number of desorption steps of other 86 metal ammine complexes were given in the annex of the study. In 2010 and 2011, ammonia dynamics of $Mg(NH_3)_6Cl_2$ were investigated by Tekin et al. with the help of DFT and neutron scattering techniques [11, 12]. These studies include crystal structure predictions carried out with CASPESA (details will be given in Methods section) and comparison of ammonia dynamics obtained from neutron scattering and DFT.

Furthermore, Westman et al. examined two calcium chloride ammines which are $Ca(NH_3)_2Cl_2$ and $Ca(NH_3)_8Cl_2$ in order to have a better knowledge about these structures [13]. In this study, X-ray powder diffraction was used to investigate formation and decomposition of the structures and symmetries were reported to be *Pnma* for calcium octaammine and *Abm2* for calcium diammine. It was also stated that $Ca(NH_3)_8Cl_2$ were obtained to have a distorted $(NH_3)_6$ in triangular prism and irregular two ammonia molecules; whereas, it is octahedron in $Ca(NH_3)_2Cl_2$ [13].

1.3 Compuational Details

In this study, first crystal structure prediction of $Ca(NH_3)_nCl_2$ for n = 8, 6, 4, 2, 1; was carried out by CASPESA (Crystal Structure Prediction via Simmulated Annealing) [14-16] which was developed by A. Tekin and his working group.

CASPESA based on simulated annealing method, conducts global opitimization and make crystal structure more stable via increasing number of pre-defined formations. In order to run CASPESA global opitimizations, first the studied system must be parameterized. For example, for $Ca(NH_3)_8Cl_2$, $Ca(NH_3)_6$ complex can rotate and move invidiually. Three euler angle parameters (α, β, γ) were used for rotations. Chlorine atoms were only allowed to translate so only three extra parameters were defined for each Cl. For free NH_3 within the complex, additional six parameters were used for rotation and movement, seperately. At least one parameter was identified for unit cell vector depending on the crystal system. In total, 22 to 30 parameters were used for $Ca(NH_3)_8Cl_2$. Moreover, N-Ca (4.0 - 4.75 Å), and H-Cl (2.4 - 3.0 Å) distances were employed as objective functions for the structures with free ammonia (Only H-Cl objective function was used for the other cases).

The outcomes of CASPESA were further relaxed at the DFT [17-20] level by using plane wave DACAPO code with revised Perdew-Burke-Ernzerhof (RPBE) exchange-correlation functional [21, 22] including 340 eV cut off energy for the plane waves and 500 eV for density grid. The Brioullin zones were obtained via expanding k-points starting from 2x2x2.

The resulting ab-initio crystal structures were used to investigate ammonia dynamics via nudged elastic band (NEB) method. NEB was applied to examine transition position of the ammonia and the calcium ammine complex from predicted initial to final state and the minimum energy path for this transition [23, 24]. Therefore, the initial and the final states of the calcium ammine complexes were optimized at first and then used together for identifying possible intermediate states by linear interpolation. At least seven and at most nine images were used for the NEB calculations. Moreover, in some cases, climbing image was applied to move the location of the image to the saddle point (detailed information is given in Methods section).

1.4 Subject and Scope

Electricity has been taking huge part among the other forms of energy consumption in the world for many decades. Besides, evolution of the power systems started from small isolated networks now have reached to integrated national and even international markets [25].

According to International Energy Outlook 2016 (IEO2016), world's net electricity generation will be increased by 69% in 2040, from 21.6 trillion kilowatts (kWh) in 2012 to 25.8 trillion kWh in 2020 and 36.5 billion kWh in 2040 [25].

In the early 2000s, greenhouse effect on environment caused a common attention for development of renewables. Nevertheless, coal has met approximately two third of the world fuel requisite for electricity production since 1980s, it is estimated in IEO2016 that there will be a momentous change in the fuel type for the production of electricity (Figure 1.1) [25].

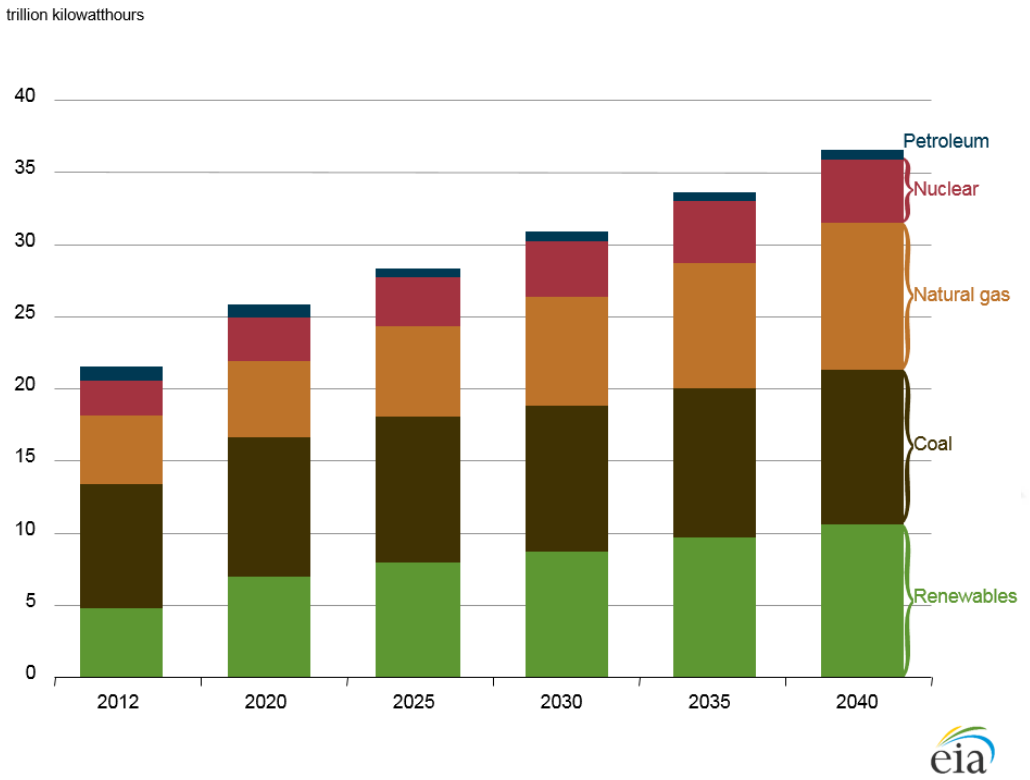

Figure 1.1: World net electricity generation by fuel-IEO2016.

As it is seen in Figure 1.1, coal margin in total generation declines from 40% in 2012 to 29% in 2040, even as coal-fired generation rises by 25% in the next 23 years. Meanwhile, the percentage of the production for the renewable energy sources is expected to grow from 22% to 29% by 2040 [25].

Following renewables, natural gas and nuclear power are the other leading sources of electricity production with a raise of 2.7% per year for natural gas and 2.4% per year for nuclear, respectively. Considering coal burning sources very slightly increase in regard to IEO2016 projection, renewables pass coal and take the first place in electricity production of the world by 2040 [25].

Figure 1.2 indicates that, renewable energy sources represent an increasing share of total global electricity supply, and are the fastest growing source of the electricity generation [25].

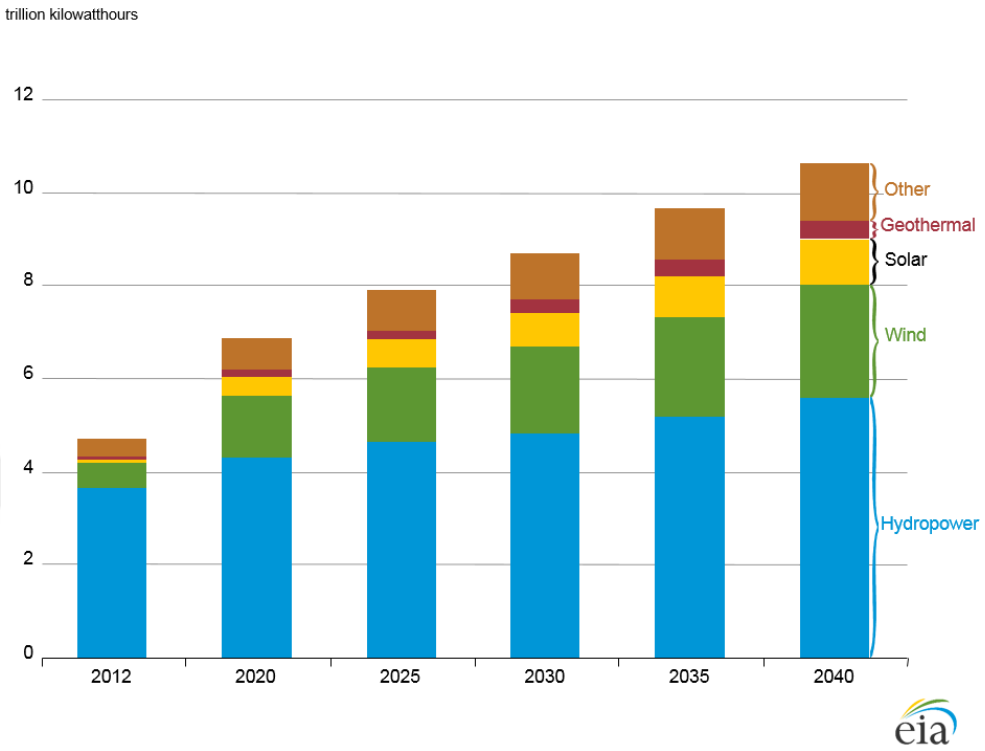

Figure 1.2: World net electricity generation from renewable-IEO2016.

Within the period 2012-2040, overall production of renewables goes up by 2.9% per year in keeping with its rise in the global electricy generation from 22% to 29%. The nonhydropower renewable energy production is the leading source of the growth among the others, which boosts just over an average 5% per year and surpasses raise in natural gas (2.7% per year), nuclear (2.4% per year) and coal (0.8% per annum). Among the addition of the 5.9 trillion kWh renewable new generation during this forecast, hydroelectric power and wind each represent 1.9 trillion kWh (33%), solar energy 859 billion kWh (15%) and other renewables (mostly biomass and waste) 856 billion kWh (14%) [25].

According to IRENA report [26] in 2030, renewable share for energy consumption will grow approximately between 20% and 70% in many countries. In some developed countries, renewable energy is on the rise and most of them have the potential to follow this substantial increase. Moreover, energy demand in developing countries is growing and leading more accessibility for renewables, countries tend to invest more on

efficient clean energy technologies for environmental issues and reduce their dependency on non-renewable sources at the same time [27, 28].

In todays' world of transition to renewables, hydrogen, as being one of the renewable fule of the future, is an important energy transport material and alternative for fulfilling this energy demand. Hydrogen, as a clean energy source, has no green house effect. Furthermore, it has a high efficiency and limitless source. Hydrogen has been talked for many years, yet there is not enough significant progress for its deployment or extensive use among other renewables. Despite those advantages, storage and production are still a problem preventing widespread use hydrogen fuel technology [29-31].

The most environmentally friendly way to produce hydrogen can be achieved with decomposition of water to hydrogen and oxygen by solar-powered electrolysis. This can be feasible only if tandem cells to be used in a cheap and convenient way [32, 33]. The burning step can be carried out by using alkaline electrolyte polymer electrolyte membrane (PEM) fuel cells. The most difficult of these steps is the storage of hydrogen and this project focuses on this point.

Hydrogen can be stored and transported in gas and liquid phases [33, 34]. However, hydrogen storage and usage in gas phase requires quite large volumes. Storing in liquid phase needs operation condition under high pressures and a part of produced energy is used liquefaction process. It is also possible to store hydrogen in the solid phase. For this purpose, metal hydrides [35, 36], carbon nanotubes [37], metal-organic systems [38], metal borohydrides [39, 40], ammonium borane [41] and amide / imide [42] systems have been extensively examined. Nevertheless, there is no perfect material capable of providing fast, reversible hydrogen desorption and absorption at high densities. Considering its energy capacity and distribution infrastructure, methane and methanol are more advantageous as compared to hydrogen. Nonetheless, they cause CO_2 emission because of the carbon they contain.

In addition, ammonia can be regarded as a carbon free sole chemical energy carrier. Ammonia does not cause greenhouse effect and considering its high hydrogen density, it can be an alternative to hydrogen. Ammonia is mainly produced from natural gas, but there are also some coal-based ammonia plants started production in countries such as China.

With the help of having highly developed ammonia infrastructure and retention of CO_2 yielded from coal-based ammonia production, ammonia is an alternative source for a long-term, a lifetime of around 115 years [43], rather than being a short-term solution in transportation sector.

Due to having excessive toxicity, ammonia still is not regarded as a high potential fuel alternative. However, it has a lower degree of toxicity when stored in metal ammine complexes such as $Mg(NH_3)_6Cl_2$ [6] and $Ca(NH_3)_8Cl_2$ [10]. According to these studies [6-10], these metal ammines are practical and reversible hydrogen storage material with a gravimetric density of 10 wt%. In order to be used in Polymer Electrolyte Membrane Fuel Cells (PEMFCs), ammonia must be decomposed into nitrogen and hydrogen over a catalyst at 300 °C. Finding the appropriate catalysis for this reaction is still a big challenge preventing widespread use of ammonia.

Ammonia itself contains 17.8 wt% hydrogen and can be used directly as fuel in internal combustion engines or in Solid Oxide Fuel Cells (SOFC). As seen in Figure1.3, metal ammines have higher volumetric hydrogen density than that of liquid ammonia and other metal hydrides.

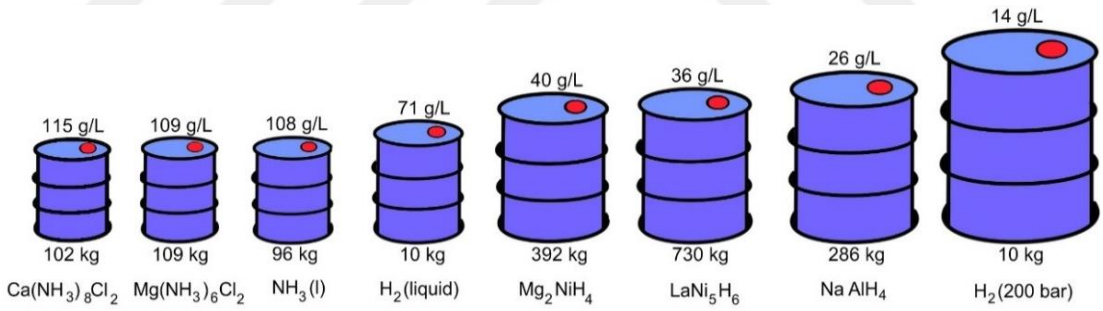

Figure 1.3: Mass and volume details of eight different materials storing 10 kg hydrogen reversibly [9].

Figure 1.3 also indicates mass comprasion of different storage methods containing same amount of hydrogen (10 kg) and it is clear that metal ammine complexes are much lighter than metal hydrides [9].

The general principle of hydrogen storage in metal ammine complexes is illustrated in Figure 1.4. The absorption of ammonia is exothermic for all salts; therefore, desorption of ammonia is endothermic and requires energy equivalent to that of released during absorption [10].

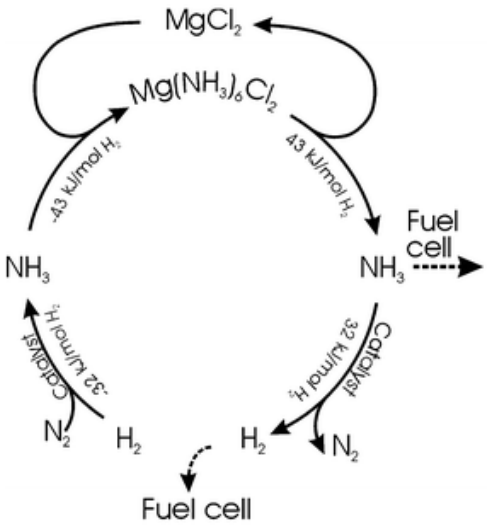

Figure 1.4: Hydrogen storage principle in metal ammine salts having a general formula $M(NH_3)_mX_m$ [10].

The most studied metal ammine salt in the literature is $Mg(NH_3)_6Cl_2$, which has a low vapor pressure of only 2 mbar at room temperature and high gravimetric (9.19 wt% hydrogen) and volumetric (109g H_2/l) hydrogen densities. $Ca(NH_3)_8Cl_2$ is also an important metal ammine salt which contains 9.78 wt% hydrogen that can be used in mobile applications. Besides, its ammonia release occurs at lower temperatures than magnesium metal ammine. Because of this low temperature ammonia release, the ammonia vapor pressure at 300 K of $Ca(NH_3)_8Cl_2$ is 0.77 bar. Another advantage of these two metal ammine salts is that of being cheap and the end product such as $MgCl_2$ and $CaCl_2$ which are abundant and non-toxic salts [44].

Temperature Controlled Desorption (TCD) experiments [9] show that ammonia releases from $Mg(NH_3)_6Cl_2$ in three-step decomposition process. As shown in Figure 1.5, firstly $Mg(NH_3)_6Cl_2$ complex releases four ammonia molecules at approximately 175 °C and forms $Mg(NH_3)_2Cl_2$ [9]. Subsequently, one ammonia molecule of this diammine complex is desorbed at 300 °C and forms $Mg(NH_3)Cl_2$. Finally, at 400 °C, the last remaining ammonia molecule is released to yield $MgCl_2$.

On the other hand, $Ca(NH_3)_8Cl_2$ releases ammonia following four-step decomposition process. At about 60 °C, the calcium octaammine salt releases four ammonia to form $Ca(NH_3)_6Cl_2$ (equation 1.1).

$$Ca(NH_3)_8Cl_2 \rightarrow Ca(NH_3)_4Cl_2 + 4NH_3(g) \quad (1.1)$$

Later at 80 °C, two ammonia molecules are released to form the diammine complex as seen in equation 1.2.

$$Ca(NH_3)_4Cl_2 \rightarrow Ca(NH_3)_2Cl_2 + 2NH_3(g) \quad (1.2)$$

As given in equation 1.3, desorption of the one of two ammonias occurs at about 200°C to form the mono ammine salt.

$$Ca(NH_3)_2Cl_2 \rightarrow Ca(NH_3)Cl_2 + NH_3(g) \quad (1.3)$$

Finally, at 250 °C, the last remaining ammonia molecule releases to yield $CaCl_2$ [9].

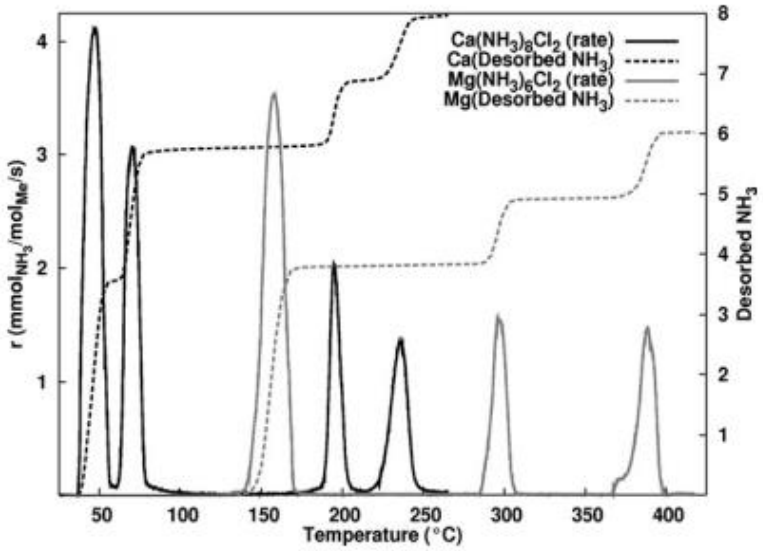

Figure 1.5: Temperature controlled ammonia desorption from $Mg(NH_3)_6Cl_2$ and $Ca(NH_3)_8Cl_2$ with a heating rate of 1°C min^{-1} [9].

Figure 1.5 also points that the calcium octaammine salt can release ammonia at a much lower temperature than that is for magnesium ammine complex. The main reason for this difference is the fact that there are two free ammonia molecules not in coordination with calcium. These free ammonia molecules tend to easily escape from the solid complex.

.

2. METHODS

2.1 Crystal Structure Prediction via Simulated Annealing (CASPESA)

Crystal structures are required for the NEB calculations. Since there is no reported experimental crystal structures for all the studied systems, first crystal structure predictions have been performed using CASPESA approach, a global crystal structure optimization method based on simulated annealing [11, 12].

In the literature, molecular diffusion of ammonia in $Mg(NH_3)_nCl_2$ n = 6, 2,1 has been studied in detail by Tekin et al. [11]. In this study, CASPESA was employed to find the crystal structure of $Mg(NH_3)_6Cl_2$ for which there is no reported experimental structure. Generally, the hydrogen bonds formed between the hydrogen atoms of NH_3 and the chlorine atoms of $Mg(NH_3)_nCl_2$ n = 6, 2, 1 make these complexes more stable. This fact can be used to construct the crystal structure by maximizing the number of hydrogen bonds in a crystal cross-sectional area of (2x2x2) by the simulated annealing method [11], using only various bond length criteria. With the help of this method, two $Mg(NH_3)_6Cl_2$ stuctures with *C2/m* and *R-3* symmetries as well as experimentally known *C2/m* and *Cmmm* symmetrical crystal structures for n = 2, 1 were reproduced. It is experimentally known that the crystal structure of $Ni(NH_3)_6Cl_2$ also has monoclinic unit cell with *C2/m* symmetry [11].

After this success, this algorithm was further used in other promising hydrogen storage materials such as metal borohydrides. For example, previously proposed tetragonal $I\bar{4}m2$ and orthorhombic *F222* symmetry structures (14.9 wt% hydrogen and approx. 9 wt% hydrogen release at 350 °C) were yielded for $Mg(BH_4)_2$ [14]. Subsequently, the same algorithm was applied to $LiBH_4$ (18.5 wt% hydrogen), the lightest metal boron hydride [15] and a new *Pnma* symmetrical structure was obtained with an energy of 9.66 kJ/mol lower than that of experimental *Pnma* structure.

Another important metal borohydride, $NaBH_4$ [16], was also investigated by CASPESA and many local minimum crystal structures have been located. The lowest

energy structure was found to be tetragonal *P4₂/nmc* and likewise $LiBH_4$, a new monoclinic *Pm* symmetrical high temperature structure yielded.

All these studies demonstrate that CASPESA approach works reliably and correctly in different systems. Therefore, in this study, CASPESA method were applied to search the crystal structures of $Ca(NH_3)_nCl_2$ n=8, 6, 4, 2, 1 for which there are only experimental knowledge for n=8 and 2 cases.

For Figure 2.1 indicates how the parameterization is carried out in CASPESA for $Ca(NH_3)_8Cl_2$,. Hexammine calcium, $Ca(NH_3)_6$, was positioned at the origin and it was allowed to rotate in any axis. The remaining two free ammonia molecules were allowed to rotate according to spherical coordinates and translate with the help of six parameters. Chlorine atoms were only allowed to translate. Crystal system was also parameterized using at least one parameter for cubic and at most nine parameters for the tricilinic cells. All these parameters were globally optimized to increase the objective function which is the number of hydrogen bonds between Cl-H.

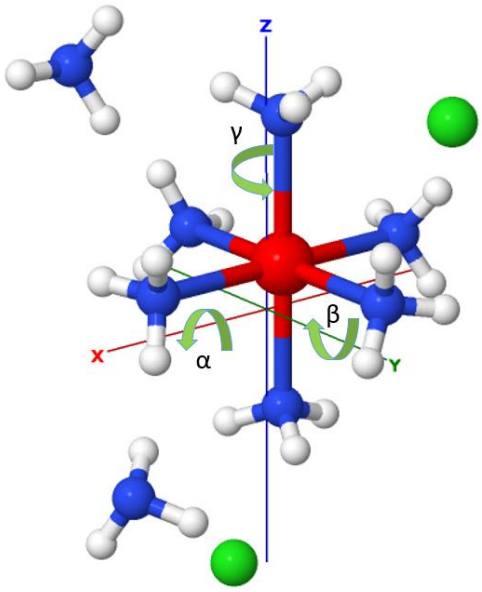

Figure 2.1: $Ca(NH_3)_8Cl_2$ as an example for CASPESA. Ca:red, N:blue, Cl:green and H:lightgrey.

Due to unemployment of any force field or DFT treatment in CASPESA, specific bond constraints were introduced to prevent atoms to get close enough to each other. More specifically, inter-atomic distances between Ca-Ca, Ca-N, Ca-Cl, N-N, Cl-Cl, H-H and Cl-N were not allowed to be smaller than 7.0 Å, 2.48 Å, 3.1 Å, 3.1 Å, 5.0 Å, 1.65 Å and 2.5 Å, respectively. These bond distance criteria were prepared with the help of

experimental $Ca(NH_3)_8Cl_2$ structure. Finally, the outcomes of CASPESA were further relaxed at the DFT level and the lowest energy structures were applied in the NEB calculations.

2.2 Quantum Mechanics

Modern electronical structure prediction is traced to Schrödinger equation postulated by Erwin Schrödinger in 1920. In general, total energy of a system can be described as seen in equation 2.1.

$$H\psi = E\psi \tag{2.1}$$

H as Hamiltionian operator represents energy of particles in a molecule and also electrostatic interaction among all these particles. *E* and Ψ describes energy and wave function, respectively. Schrödinger equation can be written for many electron atoms and molecules but only for H atom Schrödinger equation has a full solution. Althuogh it is not quite possible to solve this equation exactly, there are several approximations making this equation simpler and practical.

The first approximation is called as Born-Oppenheimer which seperates the movements of the nucleus and the electrons. This model neglects the movement of the nucleus since they are very few as compared to electrons. So that this new, mass-independent form of Schrödinger equation is called electronical Schrödinger equation.

The second approximarion is the Hartree-Fock method, in which the multi-electron wave function is written as a sum of the products of the single-electron wave functions and transformed into a determinant as known Slater Determinant (equation 2.2).

$$\psi = \frac{1}{\sqrt{\mathrm{N!}}}\begin{vmatrix} X1(1)X2(1).....XN(1) \\ X1(2)X2(2).....XN(2) \\ \vdots \qquad\qquad \vdots \\ X1(N)X2(N)....XN(N) \end{vmatrix} \tag{2.2}$$

where *N* is the number of the electrons whereas *X* refers orbitals. $\frac{1}{\sqrt{N!}}$ indicates the normalization constant.

As seen in equation 2.3 that the third approximation is to write a molecular orbital as a linear combination of atomic orbitals (LCAO).

$$\psi_i = \sum_{\mu} c_{i\mu}\phi_{\mu} \tag{2.3}$$

c represents coefficient while ϕ is atomic orbitals or basis functions. With the help of this approximation, problem does not aim to find the the best function but the best linear coefficents.

2.3 Hartree-Fock Self Consistent Field Method (HF-SCF)

Computational methods based on quantum mechanics principles solve the Schrödinger equation using the HF-SCF method to find the energies of the molecules. Since this equation is very difficult to solve, some approaches that mentioned above are applied.

As shown in equation 2.4, molecular Hamiltonian can be written in the following general form.

$$H = -\frac{\hbar^2}{2}\sum_a \frac{1}{m_a}\nabla_a^2 - \frac{\hbar^2}{2m_e}\sum_i \nabla_i^2 + \sum_{b>a}\frac{Z_a Z_b e^2}{r_{ab}} - \sum_{a,i}\frac{Z_a e^2}{r_{ia}} + \sum_{i>j}\frac{e^2}{r_{ij}} \tag{2.4}$$

In this equation, Z_a and Z_b indicate atomic numbers; whereas, *a*, *b* and *i, j* describe nuclei and electrons, respectively. The first and the second terms are the kinetic energies of nuclei and electrons, respectively. The third term is the repulsive potential energy among nuclei, the fourth one is the electrostatic interaction between nuclei and electrons, and the last one is the repulsive potential energy among electrons.

With the help of Born-Oppenheimer approach, the equation gets simplified by neglecting the first and the third terms as in equation 2.5,

$$H_{el} = -\frac{\hbar^2}{2m_e}\sum_i \nabla_i^2 - \sum_{a,i}\frac{Z_a e^2}{r_{ia}} + \sum_{i>j}\frac{e^2}{r_{ij}} \tag{2.5}$$

The hardest part of solving the Schrödinger equation is the existence of the last term, which is the electron-electron repulsion. It is very difficult to find an analytical solution for such an equation. Nonetheless, this equation can be solved by HF-SCF method and yields the wave function and energy values. According to the Hartree-Fock approach,

the multi-electron wave function is written as the sum of the products of the single electron wave functions. The electron-electron repulsive potential is calculated by considering an electron in a given orbital as being repulsed with the help of averaging potential generated by all other electrons in the molecule.

In order to perform such calculations, iterative processes called "self-consistent field" (SCF) method are performed. These operations continue to develop the orbitals in each cycle, until the energy finally reaches a constant minimum value and this latest situation is called as "self consistent field".

Energy minimization is carried out by the variational method and used the equation 2.6 as follows:

$$E_0 = \frac{\int \psi_0^* H \psi_0 d\tau}{\int \psi_0^* \psi_0 d\tau} \tag{2.6}$$

E_0 is the lowest energy and Ψ_0 refers the wave funcation at the ground state. If another wave function is used instead of Ψ_0 energy can be calculated as in equation 2.7.

$$E_\psi = \frac{\int \psi^* H \psi \; d\tau}{\int \psi^* \psi \; d\tau} \tag{2.7}$$

Energy obtained from equation 2.7 must be higher at all times than ground state energy; therefore, the variation principle is based on $E_\psi > E_0$ relation.

2.4 Ab Initio Molecular Orbital Theory

Ab Initio means that from the beginning, and it anticipates the direct application of all principles of molecular orbital theory. In fact, some approaches are used to simplify operations. However, compared to other molecular orbital methods, Ab Initio Molecular Orbital Theory is the most reliable method.

On the other hand, Ab Initio method requires a large amount of computer CPU time and hence it is not possible to apply it to very large molecules. While the number of atoms in the molecule increases, the calculations become much more difficult to solve. This theory is divided into levels based on accuracy. As the level increases, calculations become more precise and more reliable. Large molecules can only work

with low-level methods. For medium and small molecules, quite promising results can be obtained with high-level Ab Initio methods.

Computer programs dealing with the Ab Initio calculations, uses HF-SCF theory in order to solve Schrödinger equations. Nevertheless, Schrödinger equation can only be solved completely with the addition of electron correlation, configuration interaction and HF wave functions.

Energy of a HF system can be given as in equation 2.8 by simplifying the Ab Initio method:

$$E_{HF} = \sum_{\mu\gamma} P_{\mu\gamma} H_{\mu\gamma} + \sum_{\mu\gamma\lambda\sigma} P_{\mu\gamma} P_{\lambda\sigma} (J_{\mu\gamma\lambda\sigma} - X_{\mu\gamma\lambda\sigma}) + V \tag{2.8}$$

In this equation, *P* represents density matrix or density operator, *J* and *V* are the potential energy emerged from repulsion between electrons and nuclei, respectively. In order to find unknown molecular orbital coefficients shown in equation 2.3, the total energy expression is minimized according to each molecular orbital coefficient. The resulting *N* number of equations are solved with iterative cycles (*N* resembles the number of the basis functions).

2.5 Density Functional Theory (DFT)

DFT method aims to overcome the deficiencies of the HF method by slightly changing the energy expression used in the Hartee Fock method. Two new functions are used in equation 2.9, depending the total electron density (ρ). These functions are called "density functionals", which are similar to the basic functions in the Hartee Fock method [17, 18].

$$E_{DFT} = \sum_{\mu\gamma} P_{\mu\gamma} H_{\mu\gamma} + \sum_{\mu\gamma\lambda\sigma} P_{\mu\gamma} P_{\lambda\sigma} J_{\mu\gamma\lambda\sigma} + E_X(\rho) + E_C(\rho) + V \tag{2.9}$$

Differently from HF, $E_X(\rho)$ for the exchange term and $E_C(\rho)$ for the correlation term takes place in equation 2.9.

DFT has become very popular in recent years as it can be applied to larger molecules and it requires almost the same amount of computer CPU time compared to HF method. However, the most important feature of the DFT method is due to the addition of the electron correlation into its calculations. Electron correlation is by virtue of the

interactions of the electrons in a molecular system as they tend to be distanced from one another by being influenced by each other's motions [17, 18].

In the HF theory, the multi-electron wave function is expressed by Slater Determinant as a product of single electron wave functions. The DFT approach also uses single-electron wave functions. Conversely, it only tries to calculate the total electronic energy and electronic density distribution. The idea behind DFT is that there is a relationship between total electronic energy and total electron density. In 1964, Hohenberg and Kohn showed that the ground state energy and other characteristics of a system could be defined in terms of the electron density. In other words, energy (E) is a single function of ρ(r), electron density [17,18].

DFT method defines the electronic energy as the sum of several terms as given in equation 2.10.

$$E = E^T + E^V + E^J + E^{XC} \tag{2.10}$$

E^T is the kinetic energy term derived from the movement of the electrons while E^V describes the potential energy of nucleus-electron and nucleus-nucleus interactions. On the other hand, E^J and E^{XC} represents electron-electron repulsions and interactions, respectively.

As seen in equation 2.11, E^{XC} is often divided into two parts as "change" and "correlation".

$$E^{XC} = E^X(\rho) + E^C(\rho) \tag{2.11}$$

Each term in this equation is also a function. $E^X(\rho)$ is the exchange function and $E^C(\rho)$ is the correlation function.

2.6 Nudged Elastic Band (NEB)

Nudged Elastic Band (NEB) method is used for identifying the minimum energy path (MEP) connection two local minima in a potential energy surface. This technique constructs a chain of images between initial and final points by passing a saddle point where the highest energy image is located. Beside, those images have a connection to each other with the help of spring forces, which leads them to find the lowest energy along the transition path. Initial and final points of this chain often describes the energy

minima and each images between them are placed with equal spacing along the path by interpolation [23, 24].

In case the image with the maximum energy is not located at the saddle point, there is a modification of NEB called as “climbin image” used to increase energy of that image in order to move its position. In this situation, no spring forces applied along the band and the climbing image converges close to the saddle point [23].

In NEB technique, optimization of the images is carried out by spring forces and potential forces acting along the band and perpendicular to the band, respectively.

To identify the estimation of the path, several variables are defined in order to illustrate the equations. In equations 2.12 and 2.13, tangent t is used along the path; whereas, s is the parameter for the reaction path. Moreover, n represents the dimension and m+1 is the number of the images (herein after as y_i, i=0,1,…,m) used in the path [23].

$$x(s) = (x^{1}(s), \ldots, x^{n}(s))^{T} \tag{2.12}$$

$$t = (dx/ds)/|dx/ds| \tag{2.13}$$

NEB force applied on each y_i divides into two parts which are $F_{\perp}$ and $F_{\parallel}$ as shown in equation 2.14 below:

$$F_i^{NEB} = F_i^{\perp} + F_i^{\parallel} \tag{2.14}$$

The force perpendicular to the unit tangent is indicated as $F_{\perp}$ in equation 2.15,

$$F_i^{\perp} = -P_t g(y_i) \text{ with } P_t = E - t_i t_i^T \tag{2.15}$$

Gravity of the potential energy surface is described with g and P_t, as a projection operator, is defined in terms of tangent t and unit matrix E. Additionally, $F_i^{\parallel}$ which corresponds the spring force parallel to the band, is given in equation 2.16.

$$F_i^{\parallel} = k(|y_{i+1} - y_i| - |y_i - y_{i-1}|)t_i \tag{2.16}$$

In order to provide the cohesion of the chain, spring interaction is joined with a constant of k.

3. RESULTS

3.1 Crystal Structure Prediction for Calcium Ammine Complexes

In this study, first CASPESA method has been used to predict the crystal structures of calcium ammine complexes. Following the determination of the most promising structures obtained from CASPESA, DFT calculations were conducted in order to obtain energy orderings more correctly. Detailed information regarding energy and symmetry as well as comparisons to experimental findings for $Ca(NH_3)_nCl_2$ n = 8, 6, 4, 2, 1 are given below.

3.1.1 Calcium Chloride Octaammine - $Ca(NH_3)_8Cl_2$

Westman et al. [13] investigated calcium ammine complexes, $Ca(NH_3)_8Cl_2$ and $Ca(NH_3)_2Cl_2$ with the help of X-ray powder diffraction, conducted at room temperature (298K) and 1 atm pressure.

Figure 3.1 indicates the experimental and its corresponding DFT optimized structures for $Ca(NH_3)_8Cl_2$.

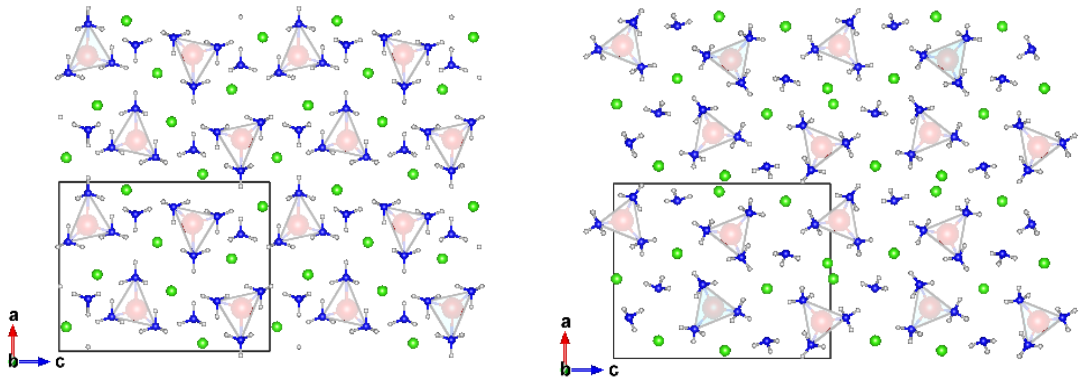

(a) Experimental Structure (b) DFT Optimized Experimental Structure

Figure 3.1: a) Experimental structure and b) its corresponding DFT optimized experimental structure of $Ca(NH_3)_8Cl_2$.

As seen in Figure 3.1 (a), in the experimental structure, six NH_3 bind to Ca atom in a trigonal prism coordination and there exits two free ammonia molecules. The experimental structure, containing four formula units in the unitcell, has a *Pnma*

symmetry (IT: 62) with the lattice parameters *a*=12.1143 Å, *b*=7.3076 Å and *c*=15.0829 Å. Even though the further DFT treatment led to the same orthorhombic *Pnma* symmetry (IT: 62), atomic positions especially those of chlorine atoms were notably changed.

Figure 3.2 highlights the coordination around Ca both in the experimental and in its DFT relaxed structures.

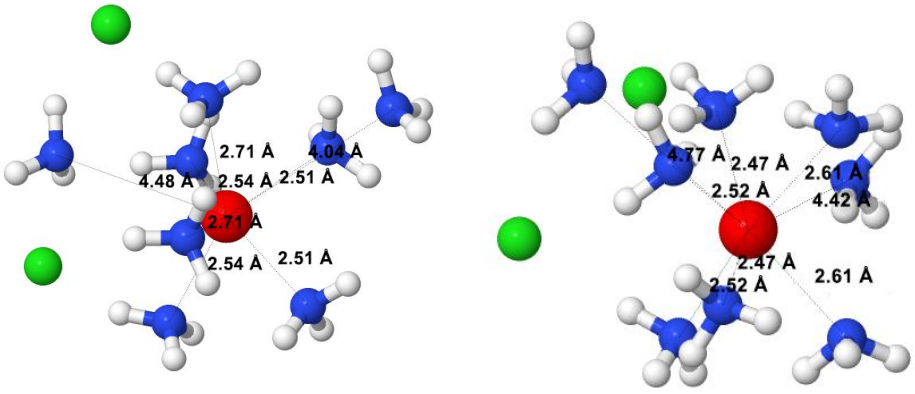

(a) Experimental Structure (b) DFT Optimized Experimental Structure

Figure 3.2: Ca-N distances in the a) experimental structure and b) its DFT optimized experimental structure of $Ca(NH_3)_8Cl_2$.

In the experimental structure, the distorted trigonal prism around Ca contains four N-Ca bond lengths are in between 2.51 – 2.53 Å and two with 2.71 Å. The closest free ammonia is 4.04 Å away from Ca atom. In the DFT relaxed structure, still the distorted trigonal prism around Ca was preserved with a slightly shortened N-Ca distances: 2.47 – 2.51 Å and 2.61 Å, respectively. Contraversily, N-Ca distance between the closest free ammonia and Ca is increased to 4.42 Å. Figure 3.3 illustrates two models including a trigonal prism and octahedral arrangements around Ca atoms used in CASPESA to predict the crystal structures of octammine complex.

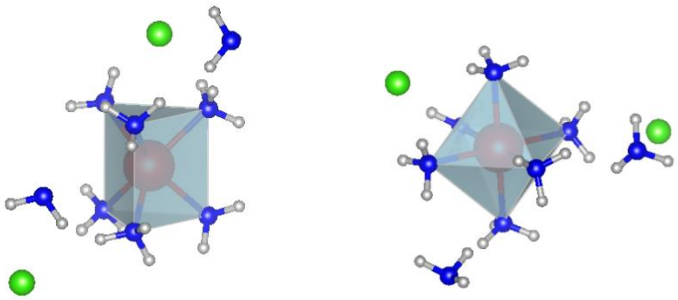

(a) Model_1 (b) Model_2

Figure 3.3: Models used in CASPESA for $Ca(NH_3)_8Cl_2$. Ca, N, Cl and H are represented by red, blue, green and lightgrey, respectively.

In both models, there are two free ammonia molecules and all six N-Ca bonds are equal in length. For each crystal system, CASPESA has been run at least 500 times starting from different initial state. The best structures obtained from CASPESA were further relaxed at the DFT level.

Figure 3.4 indicates the six DFT optimized structures lower in energy than the experimental one. All the crystallographic details and energies of these found structures were compared in Table 3.1.

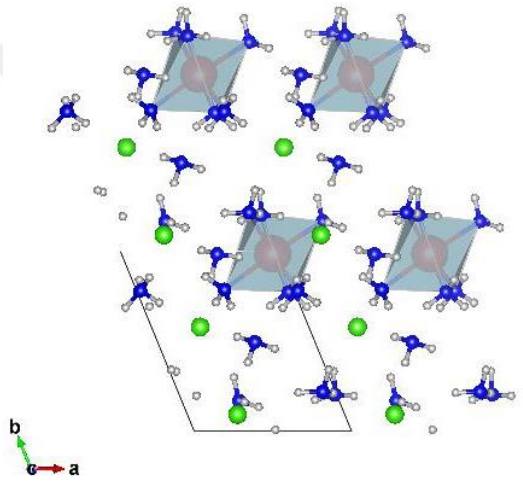

(a) CaN8_1

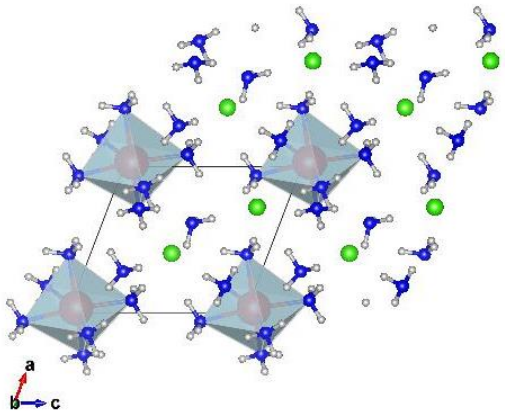

(b) CaN8_2

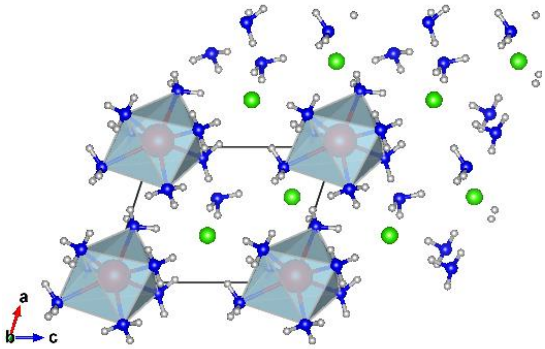

(c) CaN8_3

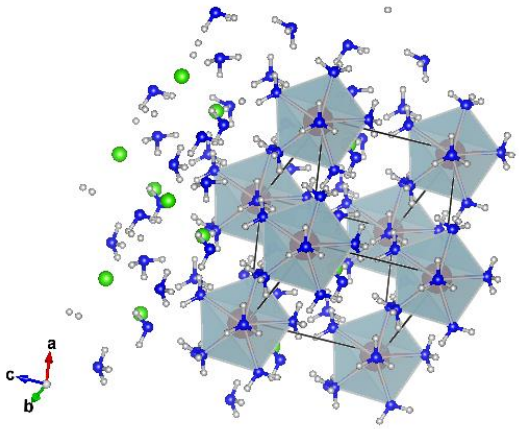

(d) CaN8_4

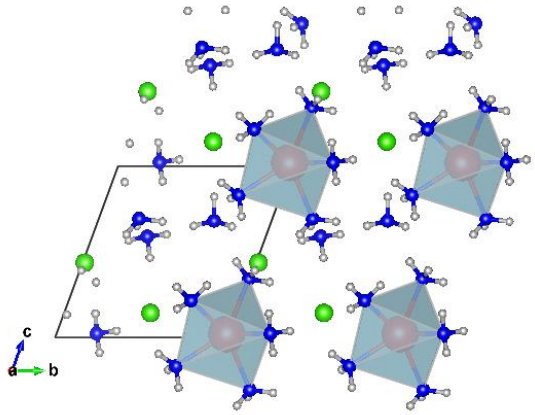

(e) CaN8_5

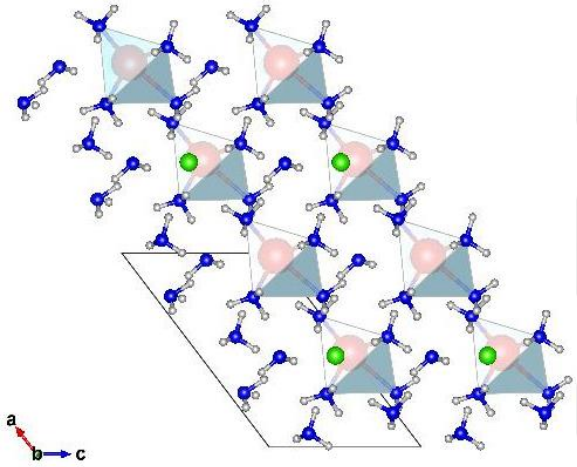

(f) CaN8_6

Figure 3.4: The lowest energy $Ca(NH_3)_8Cl_2$ structures.

As seen in Figure 3.4, the first two structures and CaN8_6 have the same octahedral coordination around Ca together with two free NH_3 molecules. Even though there is no symmetry in the five two structures (IT: 1), the latter is a monoclinic structure with *Cm* symmetry (IT: 8). Unlike the other structures, CaN8_3 forms a capped trigonal prism coordination around Ca with seven ammonia molecules. Similar to the experimental structure, CaN8_5 has a trigonal prism coordination around Ca atom. Surprisingly, even the DFT treatment started with either trigonal prism or octahedral coordination around Ca atoms, some of the found DFT optimized structures have different coordination around Ca such as CaN8_4 in which Ca has a pentagonal pyramid coordination.

Figure 3.5 shows the distances between calcium and nitrogen as well as hydrogen and chlorine atoms for the lowest energy structure, CaN8_1.

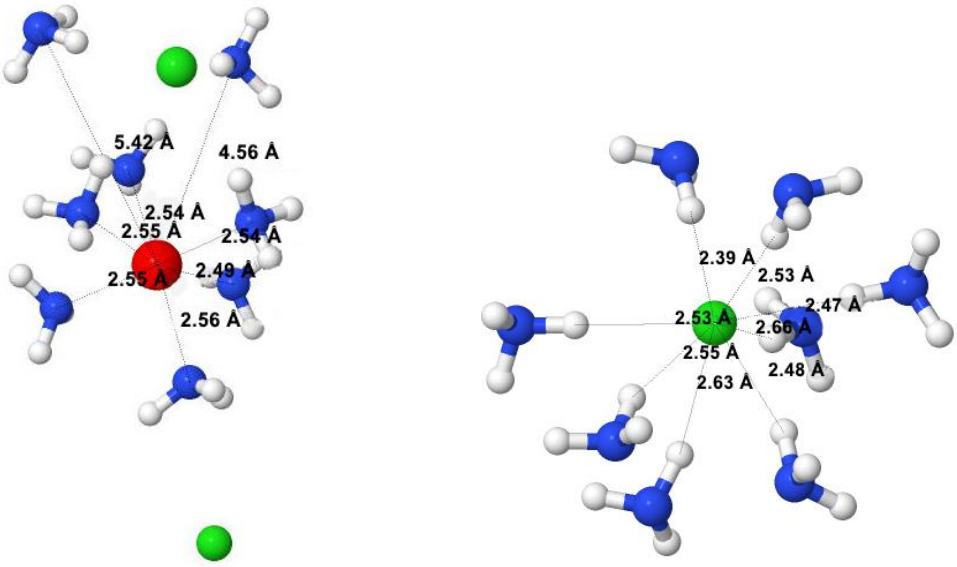

(a) l(Ca-N) (b) l(Cl-H)

Figure 3.5: Interatomic distances in CaN8_1.

In CaN8_1, N-Ca bond lengths are in between 2.49 – 2.56 Å and the closest free ammonia is 4.56 Å away from the Ca. These bond lengths are similar with that of DFT relaxed experimental structure (2.47 – 2.61 Å). On the other hand, H-Cl distances were obtained to be within the range of 2.39 – 2.66 Å. These values are quite in agreement with the H-Cl distances (2.4 – 3.0 Å) which were employed as objective functions in CASPESA. Table 3.1 gives all the crystallographic details and energies of these structures.

Table 3.1 : The crystallografic details and the total energies of $Ca(NH_3)_8Cl_2$ structures

$Ca(NH_3)_8Cl_2$	Energy(eV)	Space Group	a , b, c (Å)	α, β, γ (°)
CaN8_1	-4463.58213	*P1* (IT:1)	6.98, 8.14, 8.20	91.54, 109.07, 110.49
CaN8_2	-4463.31543	*P1* (IT:1)	7.14, 7.56, 8.27	76.04, 67.67, 80.99
CaN8_3	-4463.28963	*P1* (IT:1)	6.61, 7.56, 8.40	89.00, 71.91, 83.92
CaN8_4	-4463.19677	*P1* (IT:1)	6.81, 7.52, 7.89	94.86, 92.56, 107.01
CaN8_5	-4463.11086	*P1* (IT:1)	7.40, 7.65, 7.92	67.54, 77.69, 74.61
CaN8_6	-4462.87385	*Cm* (IT:8)	10.49, 14.07, 6.58	90.00, 127.30, 90.00
Experimental	-4460.90444	*Pnma* (IT:62)	12.11, 7.31, 15.08	90.00, 90.00, 90.00

3.1.2 Calcium Chloride Hexammine - $Ca(NH_3)_6Cl_2$

Similar to the octammine case, two models shown in Figure 3.6 consisting a trigonal prism and an octahedral were considered in CASPESA to study the hexammine calcium complex. TPD experiments [10] show that hexammine complex is not so

stable and therefore at the first ammonia release step four molecules of ammonia leaves the complex leading to $Ca(NH_3)_4Cl_2$.

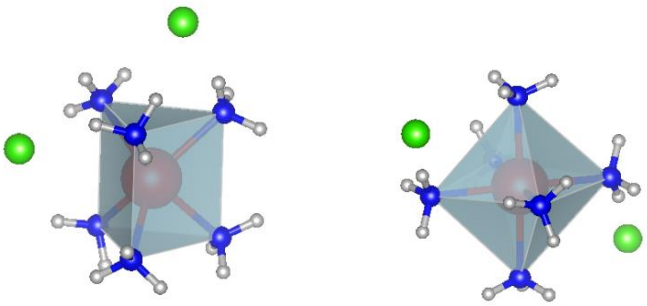

(a) Model_1 (b) Model_2

Figure 3.6: Models used in CASPESA for $Ca(NH_3)_6Cl_2$.

Figure 3.7 illustrates the DFT relaxed structures starting from the selected best CASPESA outcomes.

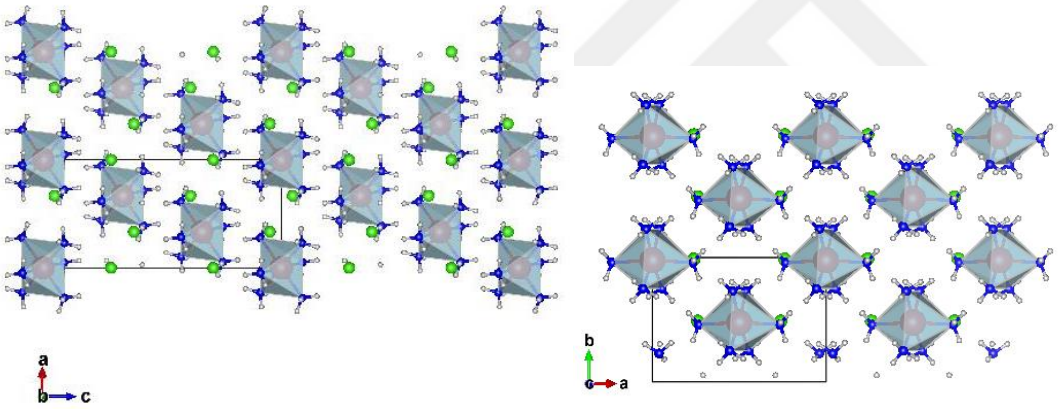

(a) CaN6_1 (b) CaN6_2

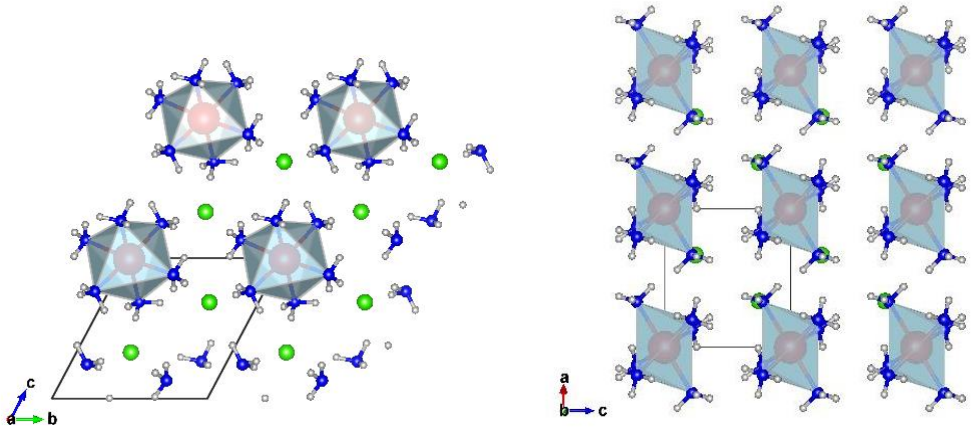

(c) CaN6_3 (d) CaN6_4

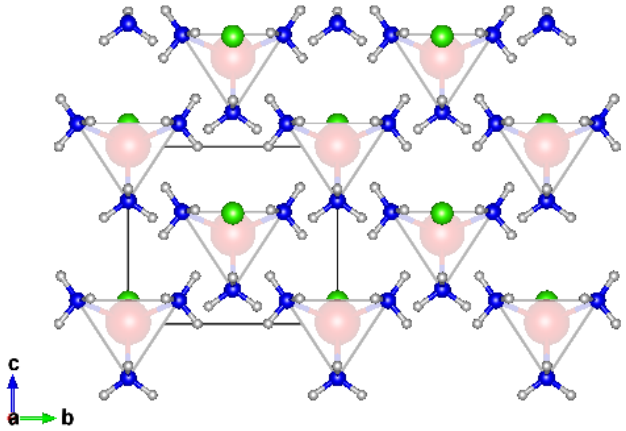

(e) CaN6_5

Figure 3.7: The lowest energy $Ca(NH_3)_6Cl_2$ structures.

In the first four structures shown in Figure 3.7, Ca prefers an octahedral arrangement. CaN6_1 has a rhombohedral cell with *R-3* symmetry (IT: 148) with cell parameters *a*=8.28 Å, *b*=8.28 Å and *c*=15.81 Å. CaN6_2 is a monoclinic structure with a *C2* symmetry (IT: 5). Among the found structures, only in CaN6_3 no symmetry has been found. The last structures, CaN6_4 and CaN6_5, have a trigonal *P321* (IT: 150) and orthorhombic *Imm2* (IT: 44) symmetry, respectively.

All the crystallographic details and energies of $Ca(NH_3)_6Cl_2$ structures were listed in Table 3.2.

Table 3.2 : The crystallografic details and the total energies of $Ca(NH_3)_6Cl_2$ structures

$Ca(NH_3)_6Cl_2$	Energy(eV)	Space Group	a , b, c (Å)	α, β, γ (°)
CaN6_1	-3822.38031	*R-3* (IT:148)	8.28, 8.28, 15.81	90.00, 90.00, 120.00
CaN6_2	-3822.32602	*C2* (IT:5)	12.98, 7.45, 8.12	90.00, 126.32, 90.00
CaN6_3	-3822.18846	*P1* (IT:1)	5.95, 7.53, 7.72	61.92, 85.09, 88.68
CaN6_4	-3822.10901	*P321* (IT:150)	7.59, 7.59, 5.98	90.00, 90.00, 120.00
CaN6_5	-3821.98331	*Imm2* (IT:44)	13.64, 7.23, 6.11	90.00, 90.00, 90.00

Figure 3.8 illustrates the distances around Ca and Cl atoms in the lowest energy structure, which is CaN6_1. In CaN6_1, three N-Ca bond lengths are 2.53 Å and the other three with 2.56 Å. Moreover, H-Cl distances were found to be in between 2.45–2.89 Å and in the range of the H-Cl objection function values (2.4 Å – 3.0 Å) used for in CASPESA.

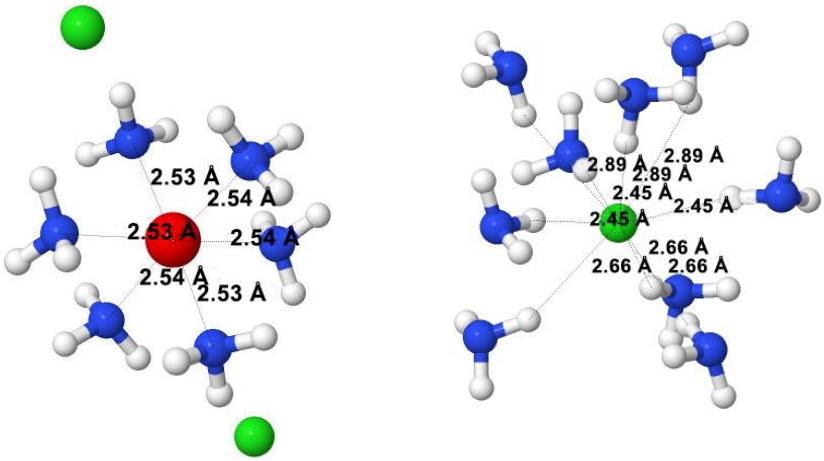

(a) l(Ca-N) (b) l(Cl-H)

Figure 3.8: Interatomic distances in CaN6_1.

3.1.3 Calcium Chloride Tetrammine - $Ca(NH_3)_4Cl_2$

Similar to hexammine case, there is no any reported experimental crystal structure for tetrammine complex even though the TPD experiments show that it is a stable phase. Therefore, it is necessary to employ CASPESA to obtain the possible tetrammine phases to be used in the NEB calculations for finding the bulk diffusion barriers. For this purpose, as given in Figure 3.9, two models were determined for crystal structure prediction of $Ca(NH_3)_4Cl_2$.

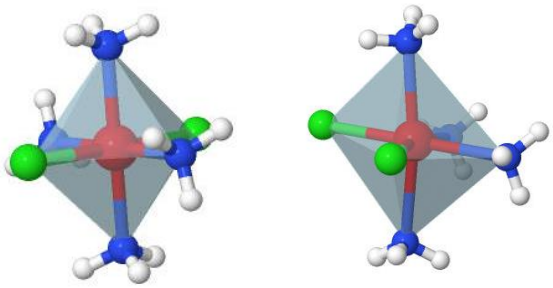

(a) Model_1 (b) Model_2

Figure 3.9: Models used in CASPESA for $Ca(NH_3)_4Cl_2$.

Both models have an octahedral coordination around Ca with four ammonia and two chlorine atoms, which are in the axial positions. The only difference between the models is the spatial arrangement in ammonia and chlorine groups: in the former chlorine atoms are positioned far away from each other; on the other hand, in the latter they are put close to each other.

Figure 3.10 shows the DFT tretaments for the best structures obtained from the CASPESA step. In particular, four structures have been located and their crystallographic details and total energies were listed in Table 3.3.

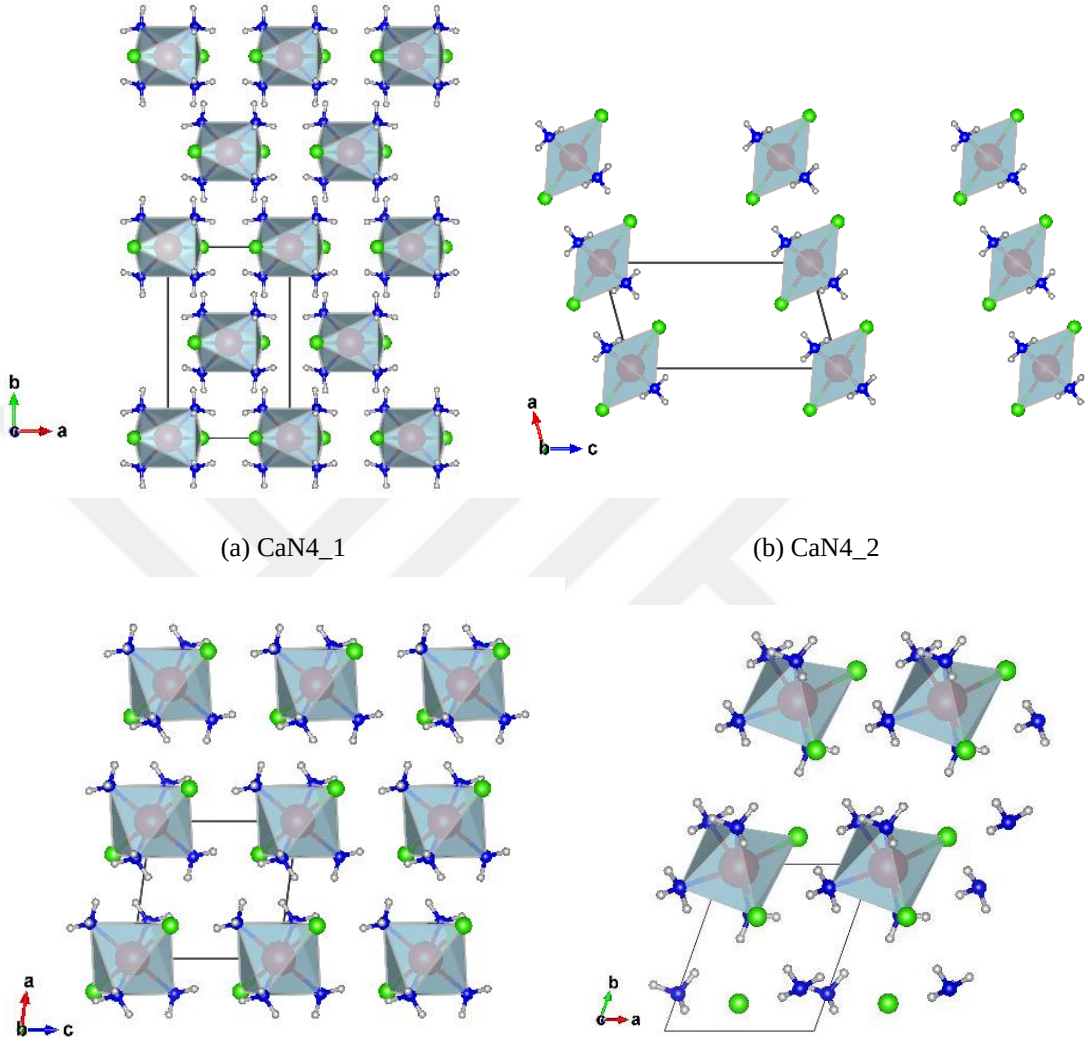

(a) CaN4_1 (b) CaN4_2

(c) CaN4_3 (d) CaN4_4

Figure 3.10: The lowest energy $Ca(NH_3)_4Cl_2$ structures.

Table 3.3 : The crystallografic details and the total energies of $Ca(NH_3)_4Cl_2$ structures

$Ca(NH_3)_4Cl_2$	Energy(eV)	Space Group	a , b, c (Å)	α, β, γ (°)
CaN4_1	-3180.91740	*C2/m* (IT:12)	6.80, 10.50, 6.58	90.00, 99.79, 90.00
CaN4_2	-3180.88519	*P2/m* (IT:10)	6.06, 8.05, 11.51	90.00, 105.21, 90.00
CaN4_3	-3180.81223	*P-1*(IT:2)	6.29, 6.62, 7.12	68.13, 80.28, 83.26
CaN4_4	-3180.80801	*P1* (IT:1)	6.49, 6.90, 7.19	83.08, 63.40, 69.49

After the DFT relaxation, all structures have an octahedral coordination around Ca atoms similar to the CASPESA models. For the first three structures, two chlorine atoms are located in the axial position and four ammonia molecules arranges

equatorially around the calcium atom. Among the found structures, CaN4_1 and CaN4_2 tends to have a monoclinic crystal system with a symmetry of *C2/m* (IT:12) and *P2/m* (IT:10), respectively. The remaining structures have a triclinic symmetry. In CaN4_4, there is one chlorine atom and ammonia molecule in the equatorial position bound to Ca atom. Figure 3.11 illustrates the distances around Ca and Cl atoms in the lowest energy structure, CaN4_1.

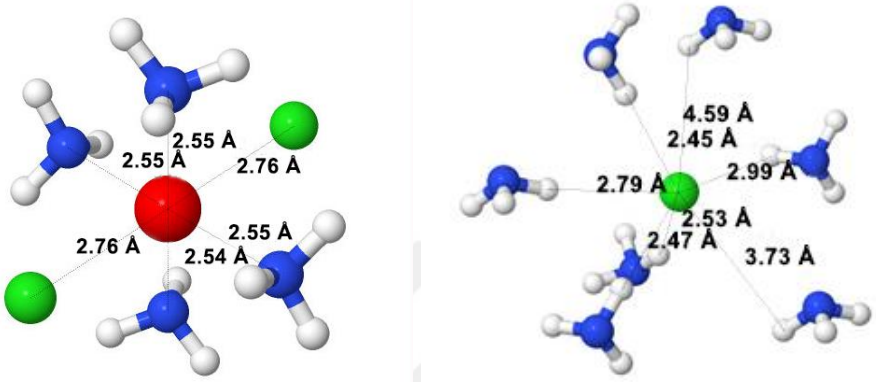

(a) l(Ca-N) (b) l(Cl-H)

Figure 3.11: Interatomic distances in CaN4_1.

As seen in Figure 3.11, N-Ca distances are almost the same and found to be 2.55 Å for three of them and one with 2.54 Å. The distances between Cl atoms were equalized to be 2.76 Å. H-Cl distances, on the other hand, change in the range of 2.47 – 4.59 Å while they are in between 2.4 – 3.0 Å in objective function employed in CASPESA.

3.1.4 Calcium Chloride Diammine - $Ca(NH_3)_2Cl_2$

Experimental structure and its corresponding DFT optimized structure for $Ca(NH_3)_2Cl_2$ are given in Figure 3.12 below:

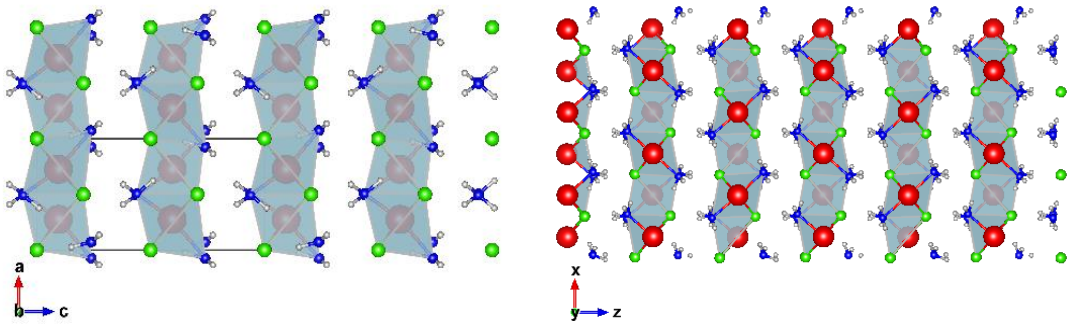

(a) Experimental Structure (b) DFT Optimized Experimental Structure

Figure 3.12: a) Experimental structure and b) its correspoing DFT optimized experimental structure of $Ca(NH_3)_2Cl_2$.

The experimentsal crystal structure for diammine complex obtained at 298 K includes four formula units of an orthorhombic cell with lattice parameters of *a*=6.0042 Å, *b*=7.8254 Å and *c*=12.3491 Å. The symmetry is broken after the DFT treatment due to the notable change in the coordinates of the atoms as shown in Figure 3.12. In the experimental structure, there is an octahedral arrangement around Ca atom together with two equatorial ammonias and four chlorine atoms.

Figure 3.13 illustrates the distances around Ca atom both in the experimental and its DFT relaxed structures.

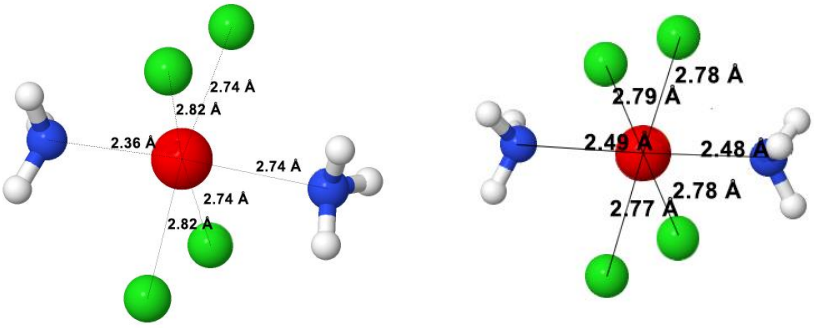

(a) Experimental Structure (b) DFT Optimized Experimental Structure

Figure 3.13: Ca-N and Ca-Cl distances in the a) experimental structure and b) its corresponding DFT optimized experimental structure of $Ca(NH_3)_2Cl_2$.

In the experimental structure, Ca-N distances are not equal: 2.36 and 2.74 Å. These distances were almost equalized in the DFT treatment to be 2.49 Å. The distances between chlorine atoms are almost the same in both structures.

Figure 3.14 shows two models used in CASPESA:

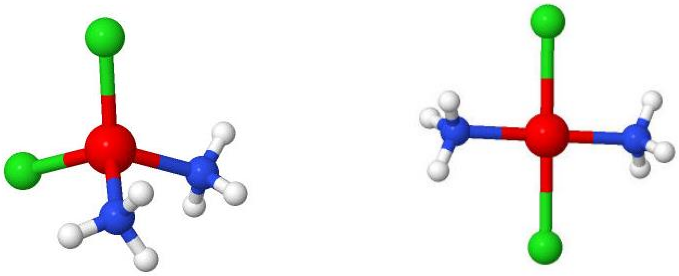

(a) Model_1 (b) Model_2

Figure 3.14: Models used in CASPESA for $Ca(NH_3)_2Cl_2$.

In the first model, there is a tetrahedral arrangement around Ca consisting of two ammonias and chlorine atoms. On the other hand, two chlorine atoms and two

ammonia molecules forms a square planar coordination around Ca atom in the second model.

Figure 3.15 shows the DFT treatments for the best structures obtained from the CASPESA step. In particular, three structures have been located and their crystallographic details and total energies were listed in Table 3.4.

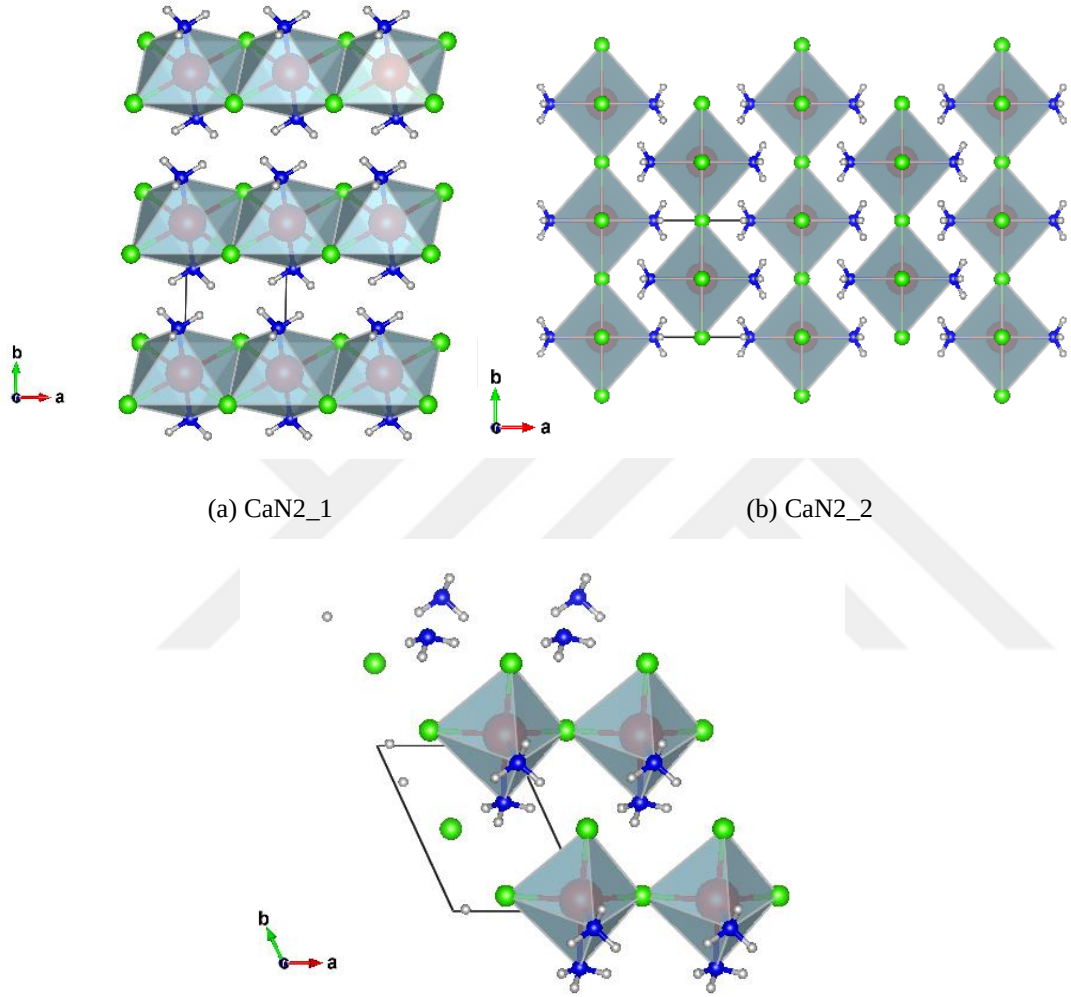

(a) CaN2_1 (b) CaN2_2

(c) CaN2_3

Figure 3.15: The lowest energy $Ca(NH_3)_2Cl_2$ structures.

Among these structures, there is an octahedral arrangement around Ca with four equatorial chlorine atoms and two axial ammonias. Two chlorine atoms are shared with neighbouring Ca atoms leading to a chain formation along 100 direction. The resulting structure has a triclinic symmetry with $P\,\bar{1}$ (IT: 2). The coordination around Ca in CaN2_2 is similar to that of CaN2_1. The only difference between them is the direction of the Ca chain, which is in 010. CaN2_2 is an orthorhombic structure with

Imm2 (IT: 44) symmetry. Unlike the other calcium diammine complexes, in CaN2_3 (no symmetry found), ammonias were bound to Ca both in axial and equatorial positions. There is a chain formation along 100 direction formed by the sharing of one chlorine atom. Table 3.4 lists the crystallografic details and the total energies of $Ca(NH_3)_2Cl_2$.

Table 3.4 : The crystallografic details and the total of $Ca(NH_3)_2Cl_2$ structures

$Ca(NH_3)_2Cl_2$	Energy(eV)	Space Group	a , b, c (Å)	α, β, γ (°)
CaN2_1	-2539.51503	*P-1*(IT:2)	4.20, 6.20, 6.68	89.52, 79.07, 88.76
CaN2_2	-2539.27884	*Imm2* (IT:44)	9.74, 5.67, 5.69	90.00, 90.00, 90.00
CaN2_3	-2539.21685	*P1* (IT:1)	4.95, 6.59, 6.89	101.23, 102.19, 111.07
Experimental	-2539.30602	*P1* (IT:1)	6.01, 7.83, 12.35	90.00, 90.00, 90.00

According to the total energies listed in Table 3.4, CaN2_1 is lower in energy than the experimental structure by 0.21 eV. Other found structures are higher in energy than the experimental one by 0.02 and 0.08 eV, respectively.

Figure 3.16 illustrates the distances around Ca and Cl atoms in CaN2_1 where N-Ca distances are almost the same 2.53 Å and 2.54 Å. The distances between Cl atoms were found to be almost the same (2.79 – 2.82 Å) and differs from each other only by 0.01 Å). H-Cl distances, on the other hand, are in between 2.71 – 3.76 Å while they are in between 2.4 – 3.0 Å in objective function employed in CASPESA.

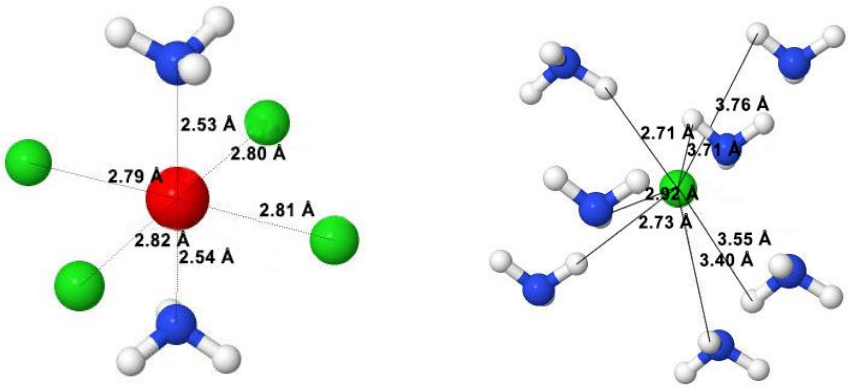

(a) l(Ca-N) (b) l(Cl-H)

Figure 3.16: Interatomic distances in CaN2_1.

3.1.5 Calcium Chloride Monoammine - $Ca(NH_3)Cl_2$

There is no any reported experimental structure for the monoamine case. Therefore, the support from CASPESA is inevitable. In CASPESA, only one model containing two formula units shown in Figure 3.17 was considered.

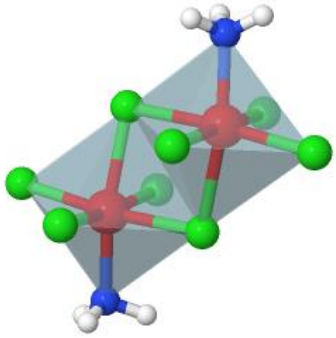

Figure 3.17: Model used in CASPESA for $Ca(NH_3)Cl_2$.

There is an octahedral coordination in this model where one NH_3 in axial position and Cl atoms in equatorial surround Ca atom. Two Cl atoms are shared with the neighbouring Ca atom. Figure 3.18 indicates the DFT treatments for the best structures obtained from the CASPESA step. In particular, two structures have been located and their crystallographic details and total energies were listed in Table 3.5.

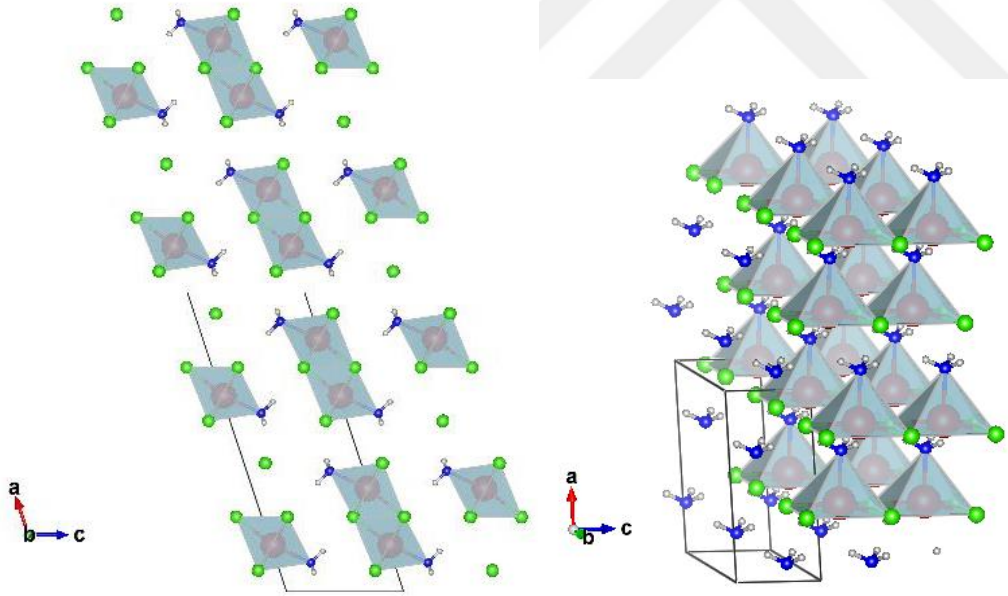

(a) CaN1_1 (b) CaN1_2

Figure 3.18: The lowest energy $Ca(NH_3)Cl_2$ structures.

In CaN1_1, there is an octahedral coordination around Ca containing five chlorine atoms and one axial ammonia. Three chlorine atoms are shared between the neighbouring Ca atoms leading to a chain formation along 010 direction. As different from CaN1_1, Ca prefers a square pyramidial coordination with four chlorine atoms

and one axial ammonia in CaN1_2 structure. Two chlorine atoms are shared in this structure leading to chain along 001 direction.

The crystallographic details and the total energies of the found structures were listed in Table 3.5. Both monoammine structures are monoclinic with a space group of *C2/m* (IT: 12) and *Cm* (IT: 8). CaN1_1 is lower in energy than CaN2_2 by 0.24 eV.

Table 3.5 : The crystallografic details and the total energies of $Ca(NH_3)Cl_2$ structures

$Ca(NH_3)Cl_2$	Energy(eV)	Space Group	a , b, c (Å)	α, β, γ (°)
CaN1_1	-2218,64905	*C2/m* (IT:12)	19.17, 4.19, 7.13	90.00, 108.35, 90.00
CaN1_2	-2218,41291	*Cm* (IT:8)	9.03, 8.97, 4.06	90.00, 94.61, 90.00

Figure 3.19 illustrates the distances around Ca and Cl atoms in CaN1_1. For this structure, N-Ca distance were found to be 2.52 Å. The distances between Cl atoms were found to have almost 0.1 Å difference to each other (2.84 Å, 2.85 Å and two with 2.75 Å). H-Cl distances, on the other hand, are in between 2.78 – 3.97 Å while they are in between 2.4 – 3.0 Å in objective function employed in CASPESA.

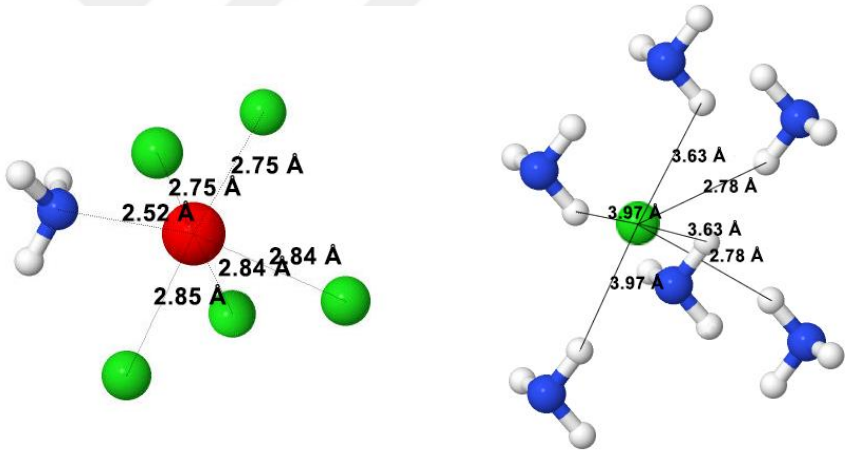

(a) l(Ca-N) (b) l(Cl-H)

Figure 3.19: Interatomic distances in CaN1_1.

3.2 Ammonia Dynamics in Calcium Ammine Complexes

Metal ammine complexes exhibit fast ad- and absorption ammonia dynamics. Depending on the temperature and pressure octammine calcium complex starts to release ammonia forming di- and monoamine complexes. At this stage, a question arises: how ammonia leaves the complex? There might be three options: i) ammonia release from the surface, ii) bulk diffusion of ammonia and iii) mixed surface and bulk diffusion.

Ammitzbøll et al. [45] investigated surface adsorption in strontioum ammine complexes. Energies regarding NH_3 adsorption in the all stable sites (full coverage) of mono-, di- and octaammine were reported as 0.303, 0.360 and 0.301 eV, respectively. For half coverage case, it is 0.285 eV, 0.372 eV and 0.383 eV.

Furthermore, Çankaya [46] studied ammonia dynamics in strontium ammine complexes and energy barriers for bulk diffusion of ammonia for $Sr(NH_3)_nCl_2$ n = 8, 6, 2, 1 were calculated to be 0.47 eV, 0.60 eV, 0,61 eV and 0,65eV, respectively. In the literature, diffusion barriers in the experimental $Ca(NH_3)_nCl_2$ n = 8, 4, 2, 1 structures were examined by Sorensen et al. [10] and were found to be 0.425 eV, 0.438 eV, 0.655 eV and 0.716 eV, respectively.

In this thesis, only the second possibility has been searched using the crystal structures found in the previous section. NEB calculations have been performed to find the possible bulk diffusion pathways for calcium ammine complexes.

3.2.1 Ammonia Dynamics in octaammine complex

Ammonia dynamics in the octammine complex has been carried out using CaN8_1 structure. For the NEB calculations, first an initial and final images were created including an ammonia vacancy and the resulting images have been relaxed at the DFT level. In between these initial and final images, five-seven intermediate images have been placed using linear interpolation.

Since there are both free and bound ammonia to Ca in the complex, the bulk diffusion has been investigated by considering several possibilities such as

i) free ammonia migrates to vacant free ammonia position,

ii) bound ammonia to Ca migrates to the vacant site to be bound to the neighbouring Ca and

iii) free ammonia migrates to be bound to Ca.

Figure 3.20 shows the diffusion barrier and ammonia migration in which free ammonia moves to the vacant free ammonia position in the neighbouring formula unit. For such a path, a diffusion barrier to be 0.489 eV has been computed. The computed value 0.489 eV is so close to the experimenatally obtained desorption enthalpy to be 0.425 eV [10].

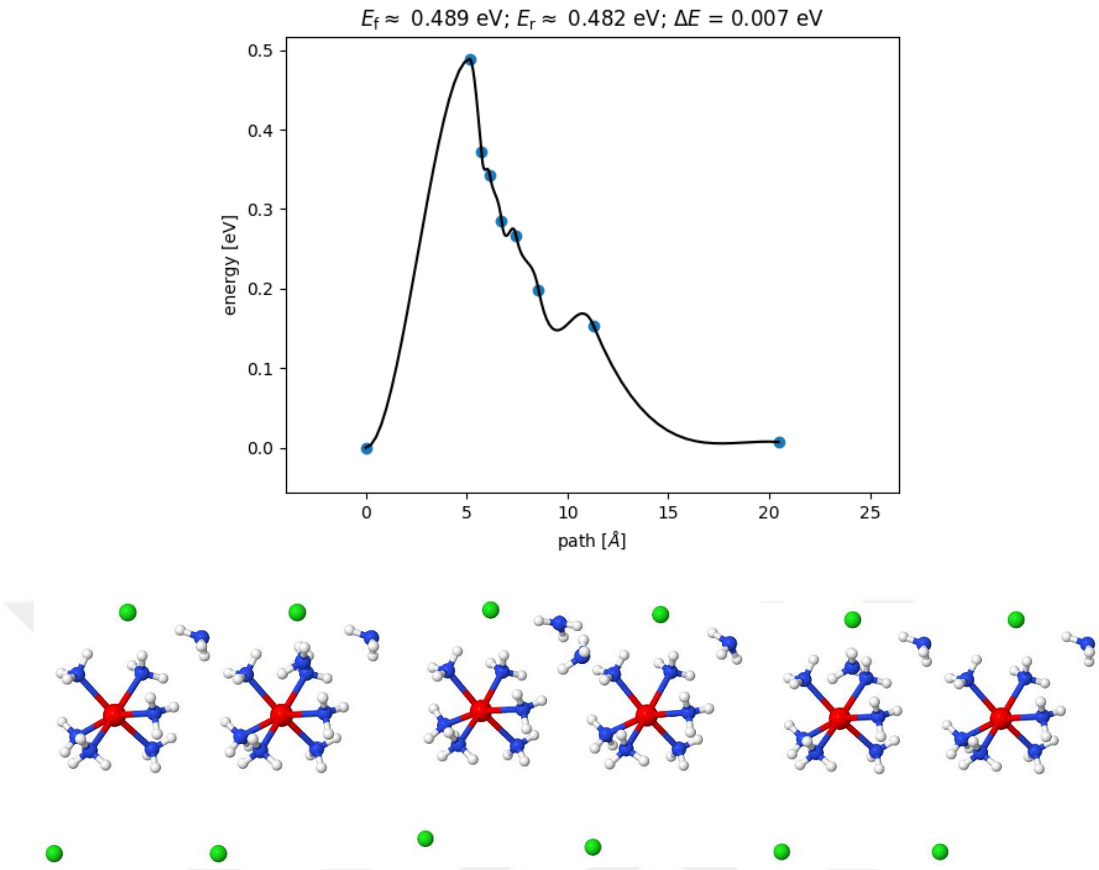

(a) Initial point (b) Saddle point (c) Final point

Figure 3.20: Ammonia dynamics in octammine: free ammonia migrates to the vacant free ammonia position.

Figure 3.21 shows the second possible ammonia migration scenario: bound ammonia moves to bound position. For this path, a barrier height was found to be 0.714 eV. This is higher than the experimental desorption barrier by 0.289 eV.

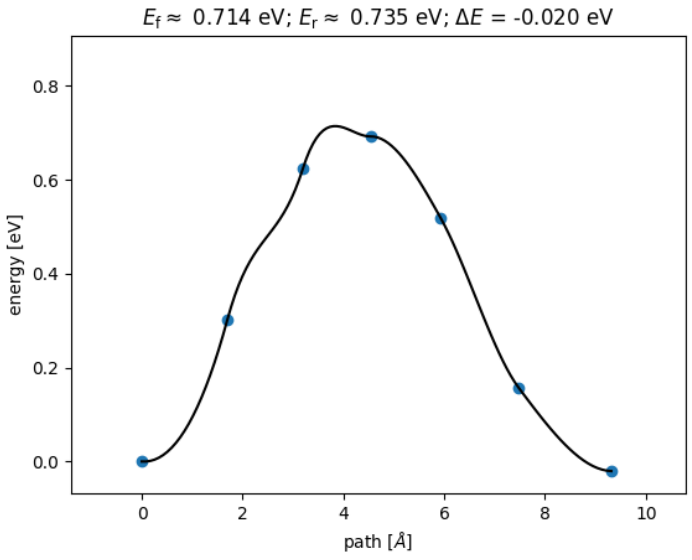

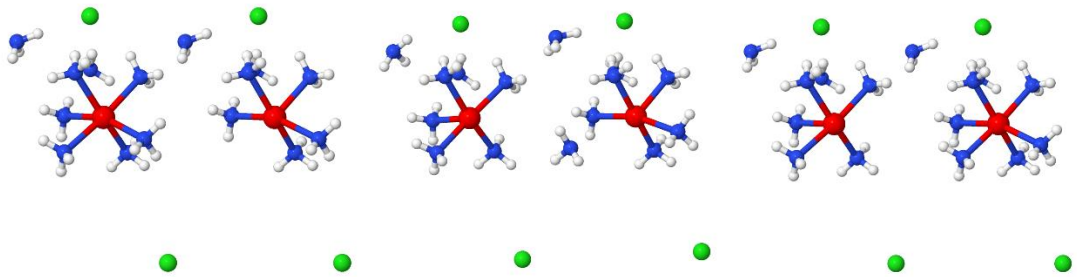

(a) Initial point (b) Saddle point (c) Final point

Figure 3.21: Ammonia dynamics in octammine: bound ammonia migrates to the vacant bound ammonia position.

Figure 3.22 shows the last possible pathway: a free ammonia moves to the position of a bounded one. The barrier height for this path was found to be 0.662 eV. As expected, it is in between the first and the second barrier heights and it is higher than the experimental desorption enthalpy by 0.237 eV.

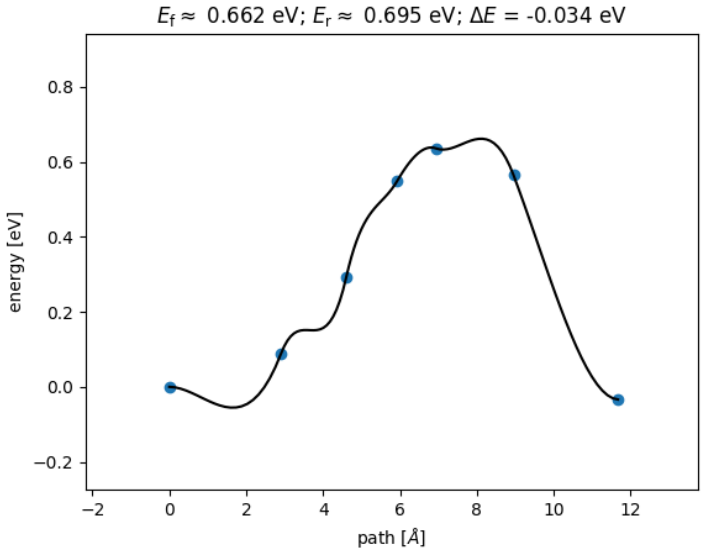

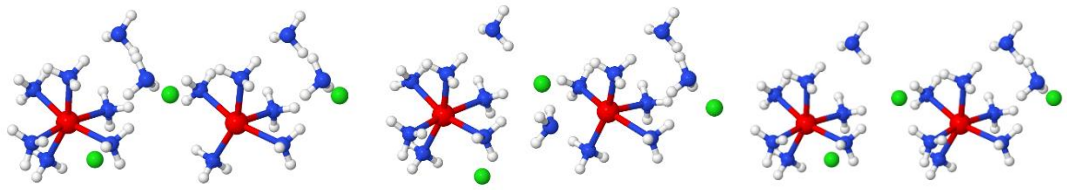

(a) Initial point (b) Saddle point (c) Final point

Figure 3.22: Ammonia dynamics in octammine: free ammonia migrates to the vacant bounded ammonia position.

All considered diffusion pathways of bulk ammonia indicate that free ammonias can easily migrate in the complex requiring an energy equivalent to the experimental desorption enthalpy. When the diffusion of a bounded ammonia is considered, barrier heights are increased by 0.2 – 0.3 eV.

3.2.2 Ammonia Dynamics in monoammine complex

To study the dynamics in the monoamine complex, the lowest energy crystal structure, CaN1_1 has been considered. Figure 3.23 shows the movement of an ammonia along the chain, which requires a barrier height of 0.735 eV. The experimentally observed ammonia desorption enthalpy in the monoamine complex is only 0.716 eV [10]. Clearly, the computed diffusion barrier is quite in agreement with the experimental value, suggesting that the bulk diffusion is possible in the monoamine case.

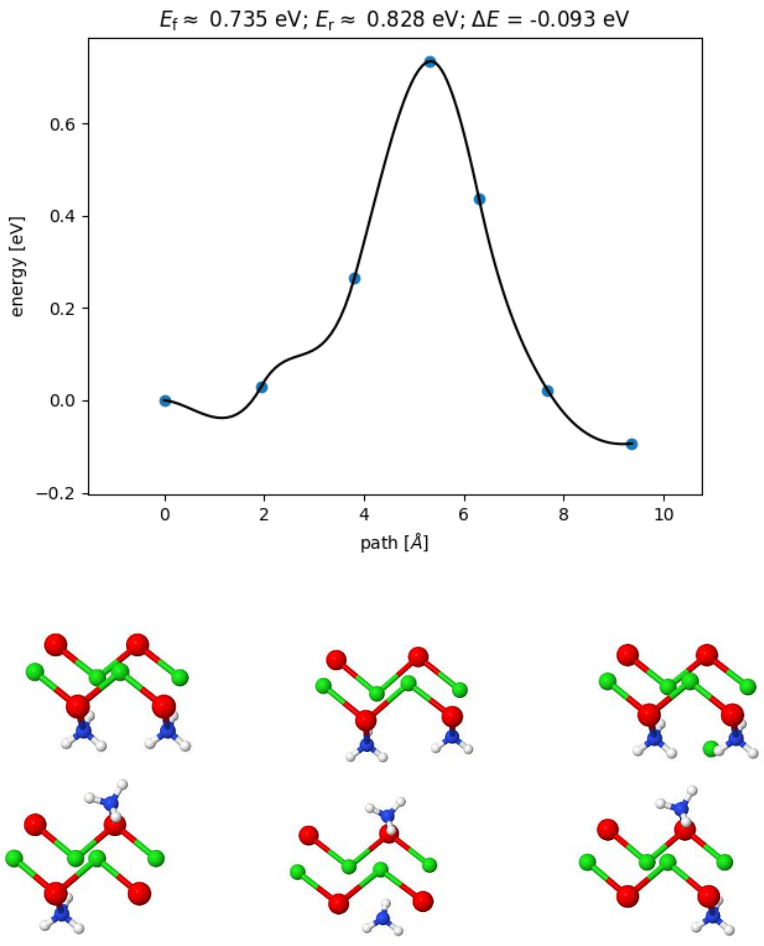

(a) Initial point (b) Saddle point (c) Final point

Figure 3.23: Ammonia dynamics in monoammine: bound ammonia migrates to the vacant bounded ammonia position.

Figure 3.24 shows both the calculated and experimental [10] desorption enthalpies obtained for calcium ammine complex were compared in Figure 3.24.

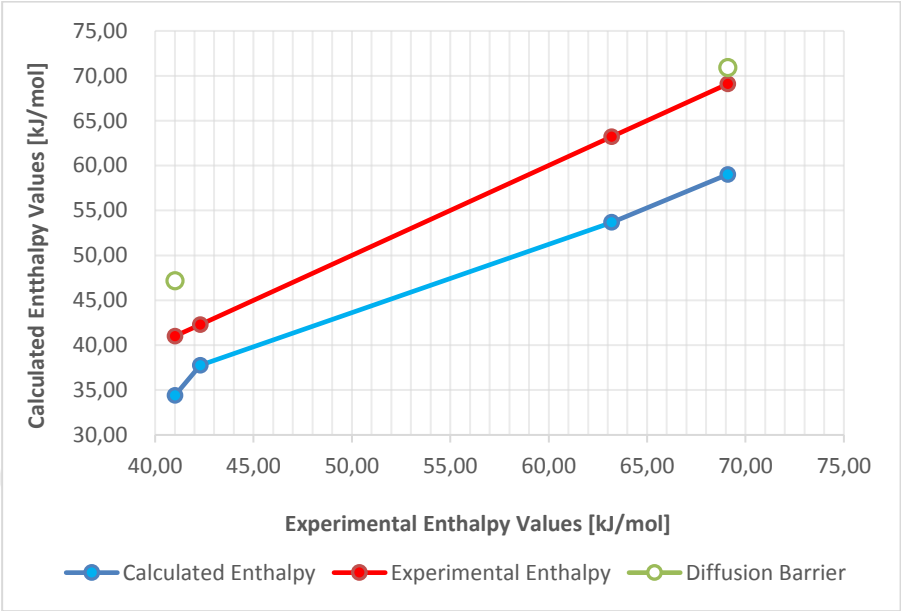

Figure 3.24: Calculated desorption enthalpies (blue) versus experimental desorption enthalpies (red) for desorption steps of 8 → 4, 4 → 2, 2 → 1 and 1 → 0 of calcium ammine. Calculated ammonia diffusion barriers are represented in green.

As seen in Figure 3.24, which also illustrates four-step decomposition of calcium ammine complex, both curves are in a very good agreement with a slightly lower for computational values, which might be fixed upon the employment of dispersion correction. Diffusion barriers, on the other hand, obtained by NEB calculations are slightly over the experimental enthalpy values.

4. CONCLUSION

This thesis aims to clarify how the fast adsorption and desorption of ammonia occurs in calcium ammine complexes. Since there is a lack of experimental crystal structures, first crystal structure predictions have been carried out by CASPESA. For each complex with a different ammonia content, new lower energy crystal structures have been found. In particular, for the octammine case a triclinic stable structure with lower in energy than the experimental one [13] by 2.68 eV has been obtained. For the found diammine structure, it is also triclinic with lower in energy than the experimental structure [13] by 0.21 eV.

Moreover, diffusion energy barriers obtained in ammonia dynamics analysis were slightly over as compared with the desorption enthalpies given in the literature [10]. Sorensen et al. reported that ammonia migration barriers of calcium octa- and monoammine were reported to be 0.425 eV and 0.716 eV at 1 bar, respectively [10]. On the other hand, energy barriers of CASPESA structures of calcium octa- and monoammine were found to be 0.489 eV and 0.735 eV. These findings indicate that bulk diffusion of ammonia in calcium complex is possible.

REFERENCES

[1] Asch, L., Shenoy, G. K., Friedt, J. M., Adloff, J. P. and Kleinberger, R. (1975). *The Journal of Chemical Physics, 62*, 2335.

[2] Jenkins, T. E. and Bates, A. R. (1981). *Journal of Physics C: Solid State Phys., 14*, 817.

[3] Schiebel, P., Hoser, A., Prandl, W., Heger, G., Paulus, W. and Schweiss P. (1993). *Journal of Physics I France***,** 3, 987.

[4] Mayer, J., Janik, J. A., Krawczyk, J., Otnes, K., Steinsvoll, O. and Stanek T. (1997). Neutron incoherent scattering study of NH3 low energy transitions in hexammine compounds, *Physica B: Condensed Matter*, *57*, 234-236.

[5] Leineweber, A., Jacobs, H., Fischer, P. and Böttger, G. (2001). Uniaxial orientational order-disorder transitions in diammine magnesium halides, $Mg(ND_3)_2Cl_2$ and $Mg(ND_3)_2Br_2$, investigated by neutron diffraction, *Journal of Solid State Chemistry***,** *156(2)*, 487-499.

[6] Christensen, C. H., Sørensen, R. Z., Johannessen, T., Quaade, U., Honkala, K., Elmøe, T. D., Køhler, R. and Nørskov, J. K. (2005). Metal ammine complexes for hydrogen storage, *Journal of Material Chemistry*, *15*, 4106-4108.

[7] Hummelshøj, J. S., Sørensen, R. Z., Kustova, M. K., Johannessen, T., Nørskov, J. K. and Christensen, C. H. (2006). Generation of Nanopores during Desorption of NH_3 from $Mg(NH_3)_6Cl_2$, *Journal of the American Chemical Society*, *128(1)*, 16-17.

[8] Jacobsen, H. S., Hansen, H. A., Andreasen, J. W., Shi, Q., Andreasen, A., Feidenhans'l, R., Nielsen, M. M., Stahl, K. and Vegge, T., (2007). Nanoscale structural characterization of $Mg(NH_3)_6Cl_2$ during NH_3 desorption: An in situ small angle X-ray scattering study, *Chemical Physics Letterrs*, *441*, 255-260.

[9] Klerke, A., Christensen, C. H., Nørskov, J. and Vegge, T. (2008). Ammonia for hydrogen storage: challenges and opportunities, *Journal of Materials Chemistry*, *18*, 2304-2310.

[10] Sørensen, R. Z., Hummelshøj, J. S., Klerke, A., Reeves, J. B., Vegge, T., Nørskov, J. K. and Christensen, C. H. (2008). Indirect, Reversible High-Density Hydrogen Storage in Compact Metal Ammine Salts, *Journal of the American Chemical Society*, *130(27)*, 8660-8668.

[11] Tekin, A., Hummelshøj J. S., Jacobsen, H. S., Sveinbjörnsson, D., Blanchard, D., Nørskov, J. K. and Vegge, T. (2010). Ammonia dynamics in magnesium ammine from DFT and neutron scattering, *Energy & Environmental Science, 3(4)*, 448-456.

[12] Churchard, A. J. et al. (2011). A multifaceted approach to hydrogen storage, *Phys. Chem. Chem. Phys.*, *13*, 16955-16972.

[13] Westman, S., Werner, P., Schuler, T. and Raldow, W. (1981). X-Ray Investigations of Ammines of Alkaline Earth Metal Halides. I. The Structures of $CaCl_2(NH_3)_8$, $CaCl_2(NH_3)_2$ and the Decomposition Product CaClOH, *Acta Chemica Scandinavica A*, *35(7)*, 467-472.

[14] Caputo, R., Tekin, A., Sikora, W., Zuttel, A. (2009) First-principles determination of the ground-state structure of $Mg(BH_4)_2$, *Chem. Phys. Lett.*, *480*, 203-209.

[15] Tekin, A., Caputo R. and Züttel, A., (2010). First-principles determination of the ground-state structure of LiBH4, *Phys. Rev. Lett.*, *104*, 215501.

[16] Caputo, R. and Tekin, A. (2011). Ab-initio crystal structure prediction. A case study: NaBH4, *J. Solid State Chem.*, *184(7)*, 1622-1630.

[17] Becke, A., D. (2014). Perspective: Fifty years of density-functional theory in chemical physics, *The Journal of Chemical Physics*, *140(13)*.

[18] Engel, E. and Dreizler, R., M. (2011). Density Functional Theory, *Theoretical and Mathematical Physics*, (1-217). Springer Berlin Heidelberg.

[19] Peterson, A. A., Abild-Pedersen, F., Studt, F., Rossmeisl, J., Nørskov, J. K. (2010). Supplementary information for "How copper catalyzes the electroreduction of carbon dioxide into hydrocarbon fuels", *Energy & Environmental Science*, *3*, 1311-1315.

[20] Kristinsdóttir, L., Skúlason, E. (2012). A systematic DFT study of hydrogen diffusion on transition metal surfaces, *Surface Science*, *606*, 1400-1404.

[21] Rappoport, D., Crawford, N. R. M., Furche, F. and Burke, K. (2009). Approximate Density Functionals: Which Should I Choose? In *Encyclopedia of Inorganic Chemistry*, John Wiley & Sons, Ltd.

[22] Hammer, B., Hansen, L. B. and Nørskov, J. K. (1999). Improved adsorption energetics within density-functional theory using revised Perdew-Burke-Ernzerhof functionals, *Physical Review B*, *59*, 7413-7421.

[23] Quapp, W. and Bofill, J., M. (2010). A Comment to the Nudged Elastic Band Method, *Journal of Computational Chemistry*, *31(13)*, 2526-2531.

[24] Henkelman, G., Uberuaga, B., P. and Jónsson, H. (2000). A climbing image nudged elastic band method for finding saddle points and minimum energy paths, *J. Chem. Phys.*, *113(22*), 9901-9904.

[25] Url-1 <*https://www.eia.gov/outlooks/ieo/electricity.cfm*>, date retrieved 02.02.2017.

[26] IRENA *(2016). Roadmap for a Renewable Future. Retrieved March 2, 2017, from* http://www.irena.org/DocumentDownloads/Publications/IRENA_REmap_2016_edition_report.pdf

[27] Adewuyia, A. O., Awodumia, O. B. (2017). Renewable and non-renewable energy-growth-emissions linkages: Review of emerging trends with policy implications, *Renewable and Sustainable Energy Reviews*, *69*, 275–291.

[28] Sena, S., Gangulyb, S. (2017). Opportunities, barriers and issues with renewable energy development – A discussion, *Renewable and Sustainable Energy Reviews, 69,* 1170–1181.

[29] Uyar, T. S., Beşikçi, D. (2016). Integration of hydrogen energy systems into renewable energy systems for better design of 100% renewable energy communities, *International Journal of Hydrogen Energy, 42(4),* 2453-2456.

[30] Zhou, L. (2005). Progress and problems in hydrogen storage methods, *Renewable and Sustainable Energy Reviews, 9(4),* 395–408.

[31] Url-2 <*https://energy.gov/eere/fuelcells/hydrogen-storage*>, date retrieved 10.02.2017.

[32] Grätzel, M., (2001). Photoelectrochemical cells, *Nature, 414,* 338-344.

[33] Riis, T., Sandrock, G. (2006). Hydrogen Storage R&D: Priorities and Gaps. In Øystein Ulleberg and Preben J.S. Vie (Corresponding authors), *Hydrogen Production and Storage* (pp.19-33). Retrieved from https://www.iea.org/publications/freepublications/publication/hydrogen.pdf

[34] Züttel, A. (2003). Materials for hydrogen storage, *Materialstoday, 6(9),* 24-33.

[35] Chen, P., Zhuc, M. (2008). Recent progress in hydrogen storage, *Materialstoday, 11(12),* 36-43.

[36] Andreasen, A., Sørensen, M. B., Burkarl, R., Møller, B., Molenbroek, A. M., Pedersen, A. S., Vegge, T., Jensen, T. R. (2006). "Dehydrogenation kinetics of air-exposed MgH_2/Mg_2Cu and $MgH_2/MgCu_2$ studied with in situ X-Ray powder diffraction", *Applied Physics A, 82(3),* 515-521.

[37] Lee, S. M., Lee, Y. H. (2000). Hydrogen Storage in single-walled carbon nanotubes, *Applied Physics Letters, 76(20),* 2877-2879.

[38] Liu, Y., Kabbour, H., Brown, C. M., Neumann, D. A. and Ahn C. C. (2008). Increasing the density of adsorbed hydrogen with coordinatively unsaturated metal centers in metal-organic frameworks, *Langmuir, 24(9),* 4772-4227.

[39] Lodziana, Z., Vegge, T. (2006). *Physical Review Letters, 97,* 119602.

[40] Hummelshøj, J. S., Landis, D. D., Voss, J., Jiang, T., Tekin, A., Bork, N., Du1ak, M., Mortensen, J. J., Adamska, L., Andersin, J. et al. (2009). Density functional theory based screening of ternary alkali-transition metal borohydrides: a computational material design project, *The Journal of Chemical Physics, 131,* 014101.

[41] Feaver, A., Sepehri, S., Shamberger, P., Stowe, A., Autrey, T. and Cao, G. (2007). Coherent carbon cryogel-ammonia borane nanocomposites for H_2 storage, *The Journal of Pysical Chemistry B, 111(26),* 7469-7472.

[42] Lohstroh, W., Fichtner M. J. (2007). Reaction steps in the Li-Mg-N-H hydrogen storage system, *The Journal of Alloys and Compounds, 332,* 446-447.

[43] World Energy Resources 2013 Survey. (2013). *Retrieved March 21, 2017, from https://www.worldenergy.org/wp-content/uploads/2013/09/Complete_WER_2013_Survey.pdf*

[44] Walker, G. (Eds.) (n.d.). *Solid-State Hydrogen Storage: Materials and Chemistry* (pp.541-549). Retrieved from http://books.google.com/books (First published in 2008).

[45] Ammitzbøll, A. L., Lysgaard, S.; Klukowska, A., Vegge, T., Quaade, U. J. (2013). Surface adsorption in strontium chloride ammines, *Journal of Chemical Physics, 138(16),* 164701/1-164701/6.

[46] Çankaya, M. (2016). Crystal Structure Prediction and Ammonia Dynamics in Strontium Ammine Complex. (Yüksek Lisans tezi). İstanbul Teknik Üniversitesi, Enerji Enstitüsü, İstanbul.

CURRICULUM VITAE

Name Surname **:** Sencer Büyükyeğen

Place and Date of Birth **:** Fatih, 26.07.1985

E-Mail **:** buyukyegen@gmail.com

EDUCATION

B.Sc. **:** 2007, İstanbul Technical University, Faculty of Science and Literature, Physics Engineering